National Technical University of Athens

Interdepartmental Program of Graduate Studies
Microsystems and Nanodevices

Master's Thesis:

Atomistic Simulations of Polydimethyl Siloxane and Polylactic Acid Polymer Systems for Directed Self Assembly Applications

Author:
Koulierakis Eleftherios

Supervisor:
Theodorou Doros
Professor

Athens, Greece
July 2016

Σε αυτόν που μοιράστηκε το φως του, ακόμα και αν υπήρξε τυφλός.

Acknowledgements

The time I spend at the laboratory of the Computational Material Science and Engineering Group (CoMSE) at the school of Chemical Engineering at the National Technical University of Athens, was very productive and I consider it as one of the most developmental experiences that I could possibly hope for. So, first and foremost, I want to gratefully acknowledge my professor Dr. Doros Theodorou, for not only giving me the opportunity to become a member of his group but also to develop and enhance my academic and career path. His attitude and scientific integrity will be exemplary for all of my future undertakings.

I would also like to express how thankful I am to the Post-Doc researcher Dr. Stefanos Anogiannakis. Dr. Anogiannakis has always been helpful and devoted a lot of his time to help me advance in the field of computational material science. His valuable assistance and contribution helped me to proceed fast and to completely understand all the topics that were related to my thesis. Each discussion with him was not only helping me to overcome the problems that occurred, but it was also a cultivating conversation that helped me to realise that each achievement (scientific or not), comes with hard work. His scientific and behavioural integrity will also be exemplary for all of my future undertakings.

I own a deep sense of gratitude to the Ph.D. candidate Mr. Panagiotis - Nikolaos Tzounis. Mr. Tzounis was immensely helpful and efficiently guided me in order to understand all the different aspects of my thesis. He also helped a me lot to get familiar with the software I used and was always a constant source of motivation. His guidance was of great importance to my work and I am thoroughly grateful to him for his valuable encouragement and practical advice.

I would also like to thank all of my fellow labmates for the stimulating discussions, for the fruitful days we were enthusiastically working together, and for all the fun we have had in the last academic year. Apart from colleagues and labmates, we have also become friends, transforming the lab into a pleasant working environment. So, I want to particularly thank, in no particular order though, the following CoMSE group members: Vassileios Georgilas, Spyros Kournopoulos, Orestis Ziogos, Andreas Balafoutis and Stefanos Konstantinopoulos. I hope that this friendship (also with Dr. Anogiannakis and Mr. Tzounis) will last and I wish them all the best.

I would also like to thank the following professors for participating as examiners of my thesis: Apostolos Kyritsis and Antonis Charalambopoulos.

Last but not least, I would very much like to thank my parents Mina and

Nikos as well as my grandparents for their lifelong and unconditional support. The scientific trip of my graduate studies comes to its end with the presentation of my master thesis. Thus, I would very much like to thank everyone else who encouraged me in the past two years.

Contents

List of Figures

List of Tables

Abstract

Lithography has been the most important technology that has revolutionized the semiconductor and data storage industry. It is used in the fabrication of integrated circuits and microchips. However, conventional semiconductor lithography techniques become very expensive and inefficient when the feature size that has to be patterned is less than 30nm. In order to cross the Rubicon of scale miniaturization, alternative methods should be studied. One of the most promising potential candidates is the Directed Self Assembly of Block Copolymers. In order to guide the selection of the most suitable Block Copolymers for Directed Self Assembly applications, apart from experimental work, there is an urgent need for computational work as well.

The Poly(dimethylsiloxane)-b-Poly(lactic acid) (PDMS-b-PLA) block copolymer is considered to be very suitable for directed self assembly applications due to its ability to self organize easily into tiny domains. A thermodynamic factor that describes the thermodynamic incompatibility between two different blocks in a block copolymer, and therefore controls the appearance of order from disorder is the Flory-Huggins interaction parameter χ. PDMS-b-PLA appears to have a value of χ significantly higher than that of other block copolymers, and thus, it will possibly enhance the Directed Self Assembly of Block Copolymers for Lithography purposes. In this work, a lot of attention is paid to estimating the χ parameter of PDMS-b-PLA. Apart from that, other volumetric, solubility and conformational properties of PDMS and PLA have been computationally studied by different simulation methods.

In the first chapter, an introduction is given to the thermodynamics of polymer blends and block copolymers. Initially, there is a description of polymer blends and block copolymers. Then, in order to describe the self assembly process in methematical and physical terms, there is a description of the Flory-Hugins interaction parameter χ that aims to provide the necessary background in order to understand its importance and the reason why it is taken very seriously when

it comes to the selection of novel materials. Finally, there is a description of the phase separation diagram where the appearance of unique phases is connected with the χ parameter and the degree of polymerization.

In the second chapter, a description is given of the directed self assembly process of block copolymers which is expected to provide an alternative avenue for extending the minimization of the scale features produced by conventional lithographic processes. For that reason, photolithography and directed self assembly processes are extensively explained. The two experimental methods that are used to direct the self assembly of block copolymers, graphoepitaxy and chemical epitaxy, are described as well.

In the third chapter, the systems that were studied in this work are described. Initially, the chemical structure, the production process and the applications of both PDMS and PLA polymers are analysed. Block copolymers that contain Si groups are expected to offer positive and significantly high values of the χ parameter, so PDMS-b-PLA and its potential use is analyzed.

In this work, we try to answer how suitable PDMS-b-PLA is by adopting a computational approach. For that reason there is a description in the fourth chapter of the atomistic simulation methods we used, namely Molecular Dynamics and Monte Carlo. These methods require an appropriate force field which is also described. Molecular Dynamics is a deterministic method were the Newton's second law plays a crucial role. On the other hand, Monte Carlo is a stochastic method based on the Metropolis algorithm.

In the fifth chapter, the presentation and a discussion of our results takes place as well. Volumetric, conformational, dynamical and solubility properties of the polymers PDMS and PLA have been studied. The Flory-Huggins interaction parameter χ and the enthalpy of mixing is also presented.

Finally, in the last chapter there is a discussion on the contribution of this work. The successful force field parametrization of the PDMS/PLA blend took place that took place in the context of this work will may trigger the computational study of others as well. For that reason, future plans and work that could benefit from this present work are presented.

Εκτενής Περίληψη στην Ελληνική Γλώσσα

Ο τίτλος της παρούσης εργασίας στην Ελληνική γλώσσα είναι: "Ατομιστικές Προσομοιώσεις Πολυμερικών Συστημάτων Πολυδιμεθυλοσιλοξανίου και Πολυγαλακτικού Οξέος για Εφαρμογές Κατευθυνομένης Αυτοσυναρμογής".

Η λιθογραφία αποτελεί μία από τις σημαντικότερες τεχνολογικές μεθόδους που έφερε την επανάσταση στην βιομηχανία των ημιαγωγών και της αποθήκευσης δεδομένων. Χρησιμοποιείται δε στην κατασκευή ολοκληρωμένων κυκλωμάτων και microchip. Ωστόσο, οι συμβατικές μέθοδοι λιθογραφίας καθίστανται ιδιαίτερα δαπανηρές και εν γένει αναποτελεσματικές όταν η κλίμακα των μεγεθών των δομών που παράγονται γίνεται μικρότερη από 30nm. Προκειμένου να διαβούμε τον Ρουβίκωνα της σμίκρυνσης των διαστάσεων, πρέπει αναμφίβολα να στραφούμε στη μελέτη καινούριων, πρωτοποριακών και εναλλακτικών μεθόδων. Μία από τις πιο υποσχόμενες εν προκειμένω υποψήφιες μεθόδους συνιστά η κατευθυνόμενη αυτοσυναρμογή συμπολυμερών. Προκειμένου να καταστεί δυνατή η εφαρμογή της καινούριας αυτής τεχνικής, η εξεύρεση και μελέτη των καταλληλοτέρων συμπολυμερών μέσω πειραματικών αλλά και υπολογιστικών μεθόδων είναι επίγουσα και ιδιαιτέρως αναγκαία.

Το συμπολυμερές Πολυδιμεθυλοσιλοξανίου και Πολυγαλακτικού οξέος (PDMS-b-PLA), φαίνεται να είναι κατάλληλο για εφαρμογές κατευθυνομένης αυτοσυναρμογής, λόγω της αξιοσημείωτής του ιδιότητας να αυτοοργανώνεται σε πολύ μικρό μήκος διαστάσεων. Ένας από τους σημαντικότερους παράγοντες που περιγράφει τη δημιουργία οργανωμένων δομών συμπολυμερών από τις άτακτες, συνιστά ο παράγοντας αλληλεπίδρασης Flory-Huggins χ. Το συμπολυμερές PDMS-b-PLA φαίνεται να έχει πολύ μεγάλη τιμή του παράγοντα χ, ιδιαίτερα σε σχέση με άλλα συμπολυμερή, κατά συνέπεια ενδέχεται να παίξει σημαντικό ρόλο στη Λιθογραφία και στη σμίκρυνση των διαστάσεων γενικότερα. Στην παρούσα μεταπτυχιακή εργασία, κεντρικής σημασίας υπήρξε ο υπολογισμός του παράγοντα χ για το συμπολυμερές PDMS-b-PLA. Εκτός αυτού, άλλες

ιδιότητες, ογκομετρικές και δυναμικές, όπως και ιδιότητες διαλυτότητας και δομής, έχουν μελετηθεί και υπολογιστεί μέσω προσομοιώσεων.

Στο πρώτο κεφάλαιο, δίνεται μια εισαγωγή στη θερμοδυναμική των πολυμερικών μειγμάτων και των συμπολυμερών. Αρχικά, λοιπόν, περιγράφεται η δομή των πολυμερικών μειγμάτων και των συμπολυμερών. Προκειμένου να επεξηγηθεί η διαδικασία της αυτοσυναρμογής, ή αλλιώς αυτοοργάνωσης, με όρους μαθηματικούς και φυσικούς, αναλύεται ο παράγοντας αλληλεπίδρασης χ. Η ανάλυση που ακολουθεί, επιχειρεί να εξηγήσει τη φυσική σημασία του καθώς και τους λόγους για τους οποίους λαμβάνεται τόσο πολύ υπ' όψιν στην επιλογή και στο σχεδιασμό συμπολυμερών για εφαρμογές στη λιθογραφία. Η κύρια σχέση, μέσω της οποίας μελετάται ο παράγοντας αλληλεπίδρασης χ είναι η ακόλουθη:

$$\Delta_{mix}H = \varphi_1\varphi_2 k_B T \frac{\chi}{v^*}$$

Στη σχέση αυτή, ο όρος $\Delta_{mix}H$ αφορά στην ενθαλπία ανάμειξης δύο υλικών, V είναι ο όγκος του σχηματιζομένου μείγματος, φ_1 και φ_2 είναι τα κλάσματα όγκου των εν λόγω υλικών, k_B η σταθερά Boltzmann, T η θερμοκρασία και v^* ο όγκος αλληλεπίδρασης των υλικών. Μέσω των προσομοιώσεων, δυνάμεθα να υπολογίσουμε την ενθαλπία ανάμειξης, ενώ οι υπόλοιποι όροι είναι γνωστοί πριν την έναρξη της προσομοίωσης, επομένως η παραπάνω σχέση δύναται να χρησιμοποιηθεί στον υπολογισμό του χ.

Όπως προαναφέρθηκε, η κατευθυνόμενη αυτοσυναρμογή των συμπολυμερών δύναται να αποτελέσει μια εναλλακτική προσέγγιση στη σμίκρυνση των διαστάσεων των δομών που παράγονται μέσω των συμβατικών λιθογραφικών τεχνικών. Για το λόγο αυτό, η διαδικασία της φωτολιθογραφίας, ως της πιο ευρέως διαδεδομένης λιθογραφικής τεχνικής καθώς και η αυτοοργάνωση των συμπολυμερών περιγράφονται στο δεύτερο κεφάλαιο. Ο όρος κατευθυνόμενη που χρησιμοποιείται εν προκειμένω δεν είναι τυχαίος και αφορά στο γεγονός ότι τα συμπολυμερή ωθούνται να αυτοσυναρμογηθούν. Η ώθηση αυτή επιτυγχάνεται μέσω δύο τεχνικών, αυτών της γραφοεπίταξης και της χημικής επίταξης οι οποίες περιγράφονται σε αυτό το κεφάλαιο.

Στο τρίτο κεφάλαιο υπάρχει μια περιγραφή των συστημάτων που μελετήθηκαν στην παρούσα εργασία. Αρχικά παρουσιάζονται η χημική δομή, η διαδικασία παραγωγής και οι εφαρμογές των πολυμερών PDMS και PLA. Βάσει μελετών, έχει εκτιμηθεί ότι τα συμπολυμερή που περιέχουν ομάδες πυριτίου έχουν υψηλό παράγοντα αλληλεπίδρασης Flory-Huggins και γι' αυτό περιγράφεται το συμπολυμερές PDMS-b-PLA καθώς και οι εφαρμογές στις οποίες ενδέχεται να παίξει σημαντικό ρόλο. Δεδομένου ότι η εκτίμηση της καταλληλότητας του εν λόγω συμπολυμερούς για λιθογραφικές εφαρμογές γίνεται στην παρούσα εργασία μέσω υπολογιστικών τεχνικών, στο τέταρτο κεφάλαιο περιγράφονται οι τεχνικές που χρησιμοποιήθηκαν. Οι μέθοδοι αυτές είναι η Μοριακή Δυναμική (MD) και η Προσομοίωση Monte Carlo (MC). Η πρώτη συνιστά

μία αιτιοκρατική μέθοδο που βασίζεται στην αριθμητική επίλυση του $2^{ου}$ νόμου του Νεύτωνα. Η μ έθοδος Monte Carlo από την άλλη είναι στοχαστική, και αυτό σημαίνει ότι υπεισέρχεται η χρήση τυχαίων αριθμών. Σημαντικό ρόλο σε αυτή τη μέθοδο έχει το κριτήριο αποδοχής Metropolis. Προαπαιτούμενο για τη χρήση και των δύο μ εθόδων αποτελεί η ύπαρξη ενός καταλλήλου πεδίου δυνάμεων το οποίο θα περιγράφει αποτελεσματικά τις αλληλεπιδράσεις μεταξύ των ατόμων και των μορίων που λαμβάνουν χώρα στην προσομοίωση.

Στο πέμπτο κεφάλαιο παρουσιάζονται και σχολιάζονται τα αποτελέσματα της παρούσας εργασίας. Για τα καθαρά συστατικά, δηλαδή για τα τήγματα PDMS και PLA μελετήθηκαν ως προς τις ογκομετρικές ιδιότητες η πυκνότητα και η ισόθερμη συμπιεστότητα. Ως προς τις ιδιότητες δομής μελετήθηκε το χαρακτηριστικό μήκος το οποίο αποτελεί μέτρο της δυσκαμψίας για μία πολυμερική αλυσίδα. Ως προς τις δυναμικές ιδιότητες, αυτές που μελετήθηκαν είναι η θερμοκρασία υαλώδους μετάβασης, ο μέγιστος χαρακτηρισ- τικός χρόνος χαλάρωσης και ο συντελεστής αυτοδιάχυσης. Μέρος του κεφαλαίου αυτού αφιερώνεται στην περιγραφή του συντελεστή διαλυτότητας Hildebrand. Στο τελευταίο κομμάτι του παρόντος κεφαλαίου, περιγράφονται οι ιδιότητες που αφορούν στο μείγμα των πολυμερών PDMS και PLA. Αυτές οι ιδιότητες είναι η Ενθαλπία ανάμειξης και ο ανάμειξης και ο συντελεστής αλληλεπίδρασης Flory-Huggins.

Στο τελευταίο κεφάλαιο που συνιστά και τον επίλογο αυτής της μεταπτυχιακής εργασίας, περιγράφονται όσα επιτεύχθηκαν. Η επιτυχής παραμετροποίηση του πεδίου δυνάμεων για το μείγμα PDMS/PLA ανοίγει το δρόμο για νέους υπολογισμούς που θα στοχεύσουν στην εκτίμηση και άλλων ιδιοτήτων, σημαντικών για την εξαγωγή συμπερασμάτων περί της καταλληλότητας του συμπολυμερούς PDMS-b-PLA για εφαρογές κατευθυνομένης αυτοσυναρμογής.

CHAPTER 1

Thermodynamics of Polymer Blends and Block Copolymers

1.1 Introduction

In order to understand the Self Assembly process in physical and mathematical terms, it is important to initially describe the thermodynamic laws that govern the appearance of order from disorder. Therefore, this introductory chapter briefly describes the fundamental theory concerning the Thermodynamics of Polymer Blends and Block Copolymers. Initially, we describe what the polymer Blends and the Block Copolymers are, and their structural difference as well. Then an analysis of the Flory Huggins interaction parameter takes place, due to its great importance to this work. Finally, after analysing the Flory Huggins Interaction parameter, there is a discussion of the Phase Diagram where the morphology and the shape of the microphase systems are connected with the degree of polymerization and the composition fractions.

1.2 Polymer Blends

A polymer blend is obtained when two or more polymers or copolymers are mixed and blended together. The new material which is the outcome of the blending process, exhibits different physical properties. Tailoring new polymeric materials that have an increased potential use for commercial applications is of great importance to modern industries, and that is the main reason why polymer blending has attracted so much attention. Furthermore, the development and commercialization of polymer blends are not as time-consuming and expensive as in the case of pure polymers.

There is a classification regarding whether the polymer blends are homogeneous, meaning they are miscible at the molecular level, or heterogenous. For instance, PEO, which stands for Poly(ethylene oxide), and PMMA, which stands for Poly(methyl methacrylate), are immiscible. On the other hand, the polymer blend that consists of PDMS, which stands for Poly(Dimethyl Siloxane), and PLA, which stands for Poly(lactic acid), is more miscible. This classification will also be discussed in detail below.

Figure 1.1: Structural representation of a polymer blend that consists of two different polymers [6].

It should be underscored at this point, that selecting correctly the polymer components is a way of manipulating the properties of the polymer blend [2]. Producing a material that is able to perform sufficiently and achieve its highest potential, is a result of knowledge of the thermal and mechanical properties of the polymer blend. Over the past years, many attempts have been made in order to develop and improve the thermomechanical properties of polymers by blending. In other words, the blend's suitability for some applications can be examined by evaluating thermomechanical properties. This work focuses on a computational study at the molecular level of the poly(dimethylsiloxane) and poly(lactic acid) blend.

1.3 Block Copolymers

When a polymer is made by linking only one type of small molecule, or monomer, together, it is called a homopolymer. When two or more different monomers unite together to polymerize, the polymer is called a copolymer. Block Copolymers (BCs) comprise chemically different polymer chains or blocks that are covalently bound together. BCs with two or three distinct blocks are called diblock copolymers and triblock copolymers, respectively. Triblocks, Tetrablocks, multiblocks, etc. also exist. A structural representation of a block copolymer, that consists of two different types of monomers A and B, is shown in the figure below:

Figure 1.2: Structural representation of a block copolymer BC that consists of two different monomers A and B.

The properties of block copolymers are similar to the properties of polymer blends, but the presence of chemical bonds between the different blocks benefits their stability and prevents their separation with the release of individual components. Due to their mutual repulsion as a result of enthalpic interactions, dissimilar BCs tend to segregate into different domain. This demixing procedure leads to organized periodic formations at the nanoscale, offering a variety of structural configurations. A structure of a PDMS-PLA diblock copolymer is shown in figure 1.3:

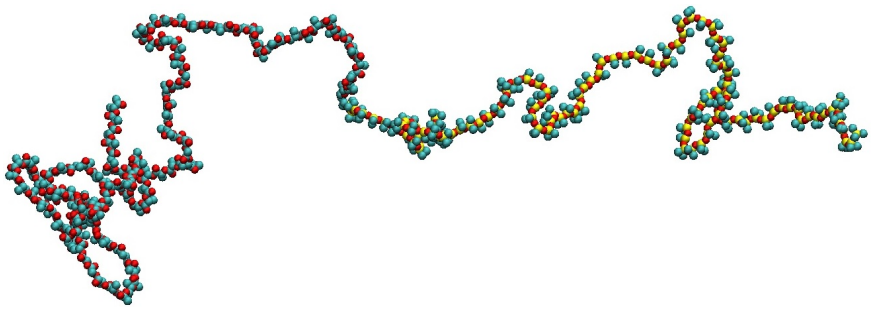

Figure 1.3: PDMS - PLA Block Copolymer structure, generated by MAPS software

Block copolymers are usually prepared by controlled polymerization of one monomer, followed by chain extension with a different monomer to form AB or

ABC block copolymers.

1.4 Flory - Huggins Interaction Parameter

The most important relationship that describes mixtures of components that are not similar is the following [34]:

$$\Delta_{mix}G = \Delta_{mix}H - T\Delta_{mix}S \tag{1.1}$$

where $\Delta_{mix}G$ is the free energy of mixing, $\Delta_{mix}H$ is the enthalpy of mixing (heat of mixing) and $\Delta_{mix}S$ is the entropy of mixing. When $\Delta_{mix}G$ is smaller than 0, then the dissimilar components are miscible. This is a necessary but not a sufficient requirement, since the expression below must be satisfied as well:

$$\left(\frac{\partial^2 \Delta_{mix}G}{\partial \varphi_i^2}\right)_{T,P} > 0 \tag{1.2}$$

In the equation above, φ_i are the volume fractions and their mathematical expression is given on equation (1.9), after introducing the entropic term in the Gibbs energy.

In order to describe the degree of miscibility we provide figure 1.4. The different degrees of miscibility are described by three different regions. The first refers to the single-phase miscible region between the two binodals. The second refers to the four metastable regions between binodals and spinodals, and the third refers to the two-phase separated regions of immiscibility, bordered by the spinodals. The figure also shows two critical solution temperatures, the lower, LCST (at higher temperature), and the upper, UCST (at lower temperature). The phase diagram with two critical points is a rule for mixtures of low molar mass components, whereas the polymer blends usually show either LCST (most) or UCST.

We observe that two regions are separated by the binodals: the metastable and the single phase region. On the other hand, the metastable region and the two-phase region are separated by the spinodals. The phase separation is governed by two thermodynamic conditions. The first refers to the spinodal:

$$\left(\frac{\partial^2 \Delta_{mix}G}{\partial \varphi^2}\right)_{p,T} = 0 \tag{1.3}$$

The second refers to the critical points:

$$\left(\frac{\partial^2 \Delta_{mix}G}{\partial \varphi^2}\right)_{p,T} = \left(\frac{\partial^3 \Delta_{mix}G}{\partial \varphi^3}\right)_{p,T} = 0 \tag{1.4}$$

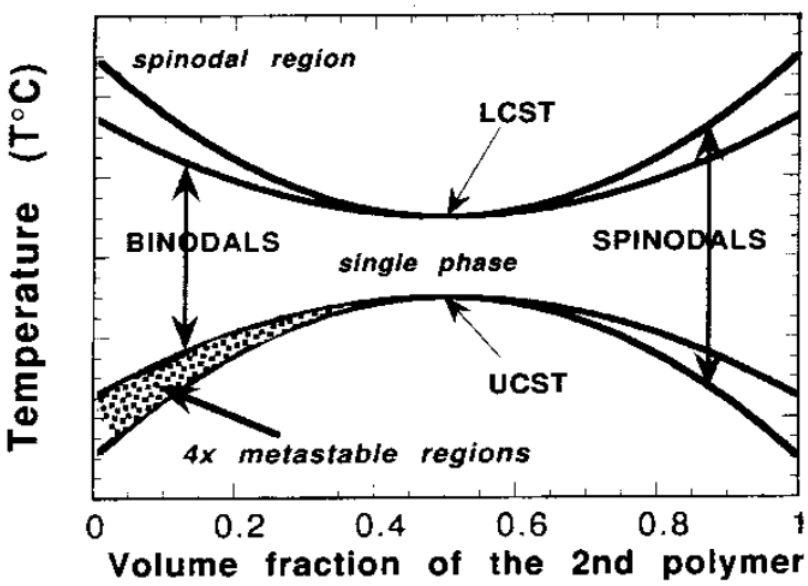

Figure 1.4: Phase diagram for liquid mixtures with the upper and the lower critical solution temperature, UCST and LCST, respectively.

Changes in composition, temperature or pressure force a single phase system to enter the spinodal or the metastable region.

The Flory-Huggins lattice theory is used to interpret polymer solutions and blends. According to this theory, the entropy of mixing is expressed by the number of rearrangements during mixing, and this is the reason why it is called combinatorial entropy. On the other hand the enthalpy of mixing is caused by interactions of different segments. The model described at this theory is a mean field model, and that is, that only average interactions are taken into account.

The most common expression of the entropy in statistical mechanics is the below:

$$\Delta_{mix} S = k \ln \Omega \tag{1.5}$$

where Ω is the number of the microstates and represents the summation of combinations of arranging N_1 and N_2 molecules into a regular lattice of N cells. N satisfies the equation above:

$$N = N_1 + N_2 \tag{1.6}$$

so that Ω becomes:

$$\Omega = \frac{N!}{N_1! N_2!} \tag{1.7}$$

By employing Stirling's approximation [1] we obtain the following expression:

$$\Delta_{mix}S = -k_B(N_1 \ln x_1 + N_2 \ln x_2) \tag{1.8}$$

where $x_i = \frac{N_i}{N}, i = 1, 2$ and k represents the Boltzmann's constant. A prerequisite for this derivation is that 1-1, 1-2, and 2-2 interactions be the same, so that all configurations of the mixed system have the same energy.

The above expression of enthalpy refers to simple or small molecules. In order to determine the enthalpy of mixing for macromolecules like polymers, it should be treated differently. Each i macromolecule ($i = 1, 2$) occupies volume V_i and the volume occupied by each monomer unit is V_{mer}. The total molecular volume, V_i, is equal to V_{mer} times the number of mer units. For solvents, the number of monomer units is 1. The volume fractions φ_1 and φ_2 are given below:

$$\begin{aligned} \varphi_1 &= \frac{N_1 V_1}{V_1 N_1 + V_2 N_2} \\ \varphi_2 &= \frac{N_2 V_2}{V_1 N_1 + V_2 N_2} \end{aligned} \tag{1.9}$$

The volume V, is given by: $V = V_1 N_1 + V_2 N_2$. It is also obvious that $\varphi_i < 1$ and $\sum_{i=1}^{2} \varphi_i = 1$. Flory has derived:

$$\Delta_{mix}S = -k_B V \left(\frac{\varphi_1}{V_1} \ln \varphi_1 + \frac{\varphi_2}{V_2} \ln \varphi_2 \right) \tag{1.10}$$

Since $\varphi_i < 1$, the $\ln \varphi_i$ value is negative, so $\Delta_{mix}S$ is positive and the product $-T\Delta_{mix}S$ in equation 1.1 has a negative contribution, thus the two polymers are more likely to be miscible.

Having finished the discussion regarding the entropic term of the equation 1.1, it is time to proceed to the enthalpic. As stated above, the entropic contribution to the equation 1.1 is always negative (favorable), but the enthalpic contribution can be ether positive or negative. Suppose we have two different segments 1 and 2 and that ε_{ij} is the energy between segments i and j.

Simple lattice models are useful for describing the mixing thermodynamics. Consider 1 lattice of total N sites and two different types of molecules 1 and 2 [23]. Each site can be occupied by only one molecule due to short-range repulsive interactions. Molecules that occupy adjacent sites interact through short-range attractive interactions. The lattice whose coordination will be denoted as z, is assumed fully occupied. The characteristic energies of nearest-neighbour attractive interactions per pair are w_{11}, w_{22} and w_{12}. These quantities are negative:

[1] Stirling's Approximation: $\ln N! = N \ln N - N$

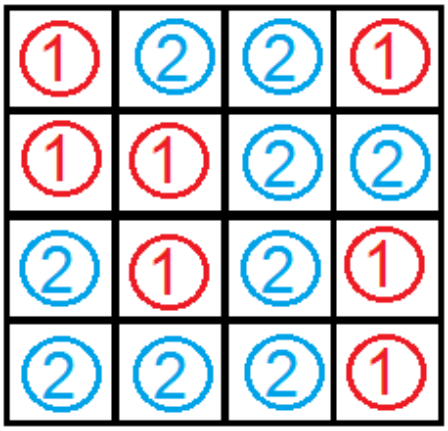

Figure 1.5: Schematic representation of simple lattice model of a binary mixture of 1 and 2 molecule types.

$$\begin{aligned} w_{11} &< 0 \\ w_{22} &< 0 \\ w_{12} &< 0 \end{aligned} \tag{1.11}$$

Full occup1ncy requires:

$$N_1 + N_2 = N \tag{1.12}$$

Let N_{11}, N_{22} and N_{12} 2e the total numbers of nearest neighbour 11, 22 and 12 pairs in this configuration. Then the total number of bonds drawn in this way is zN_1. Each nearest neighbour 11 pair carries two bonds, each nearest neighbour-12 pair carries one bond and no nearest neighbour 22 pair will carry 1 bond. As 1 result:

$$zN_1 = 2N_{11} + N_{12} \tag{1.13}$$

By repeating the connection process around 2 molecules:

$$zN_2 = 2N_{22} + N_{12} \tag{1.14}$$

In order to express the potential energy of the considered configuration we obtain:

$$E = N_{11}w_{11} + N_{22}w_{22} + N_{12}w_{12} =$$
$$\frac{zN_1}{2}w_{11} + \frac{zN_2}{2}w_{22} + N_{12}(w_{12} - \frac{1}{2}w_{11} - \frac{1}{2}w_{22}) =$$

$$E_1 + E_2 + \frac{1}{z} N_{12} w \tag{1.15}$$

where $E_1 = \frac{z}{2} N_1 w_{11}$ is the potential energy of a pure system consisting of N_1 molecules and similarly for pure 2. Then the quantity

$$w = z(w_{12} - \frac{w_{11}}{2} - \frac{w_{22}}{2}) \tag{1.16}$$

is called the interchange energy.

The relation between the exchange energy and the enthalpy of mixing is given by the relation:

$$\frac{\Delta_{mix} H}{V} = \frac{zw}{v^*} \varphi_1 \varphi_2 \tag{1.17}$$

where v^* is the interacting segment volume and is often referred to as the reference volume. It is often calculated as the square root of the product product of the individual segmental unit molecular volumes of the polymeric components ($v^* = \sqrt{V_1 V_2}$). Generally, the coordination number assumed as 8, but always must be in the range of 6 to 12. Depending on whether molecular or molar parameters are employed, the reference volume v^* represents the molecular or molar segment volumes. At this point, it is time to introduce the Flory - Huggins interaction parameter which can initially be defined as:

$$\chi = \frac{zw}{k_B T} \tag{1.18}$$

In case of molar segment volumes, instead of k we use the gas constant R. Combining 1.18 with 1.17 we obtain the useful expression:

$$\Delta_{mix} H = \varphi_1 \varphi_2 k_B T V \frac{\chi}{v^*} \tag{1.19}$$

It should also be underscored that the following expressions are equivalent with the second part of equation 1.19 :

$$\chi N_1 n_1 \varphi_2 = \chi N_2 n_2 \varphi_1 = \varphi_1 \varphi_2 k_B T V \frac{\chi}{v^*} \tag{1.20}$$

where n_i defines the number of monomers in each chain. If we also define the mass density of each pure polymer as ρ_i and the molar mass of each segment as M_i, we may obtain the following new expressions regarding the volume fractions:

$$\begin{aligned} \varphi_1 &= \frac{\frac{n_1 M_1}{\rho_1}}{\frac{n_1 M_1}{\rho_1} + \frac{n_2 M_2}{\rho_2}} \\ \varphi_2 &= \frac{\frac{n_2 M_2}{\rho_2}}{\frac{n_1 M_1}{\rho_1} + \frac{n_2 M_2}{\rho_2}} \end{aligned} \tag{1.21}$$

All the above lead to a different, yet more useful expression of the Gibbs energy of mixing per unit volume of a binary system (like the one it is studied at this work). :

$$\frac{\Delta_{mix}G}{k_BTV} = \frac{1}{v^*}\Big(\underbrace{\frac{\varphi_1}{N_1}\ln\varphi_1 + \frac{\varphi_2}{N_2}\ln\varphi_2}_{\text{entropic term}} + \underbrace{\chi\varphi_1\varphi_2}_{\text{enthalpic term}}\Big) \tag{1.22}$$

There is also another expression regarding the Flory Huggins interaction parameter, that is very useful for experimental scientists:

$$\chi = \frac{v^*(\delta_i - \delta_j)^2}{k_BT} \tag{1.23}$$

where δ_i is the Hildelbrand solubility parameter of polymer i and V_{seg} is the actual volume of a polymer segment. The Hildebrand solubility parameter provides a numerical estimate of the degree of interaction between materials, and can be a good indication of solubility, particularly for nonpolar materials such as many polymers. Materials with similar values of δ are likely to be miscible. This parameter is discussed on chapter 5.

There is a unique significance of the temperature dependant Flory Huggins parameter. It describes the free energy cost of contact between dissimilar monomers that governs the process of mixing. What needs to be emphasized is that self assembly of the polymer system occurs when χ>0. Additionally, positive values indicate an endothermic heat of mixing leading to immiscibility. Thus, negative ΔH_m values and negative or slightly positive χ values strongly indicate that the two component system is miscible. Last but not least, it should also be stated that the Flory Huggins interaction parameter itself is not a true intensive property of the system, but the deviation with v^*, ($\frac{\chi}{v^*}$) represents the interchange energy density.

So far, the discussion concerning the Flory Huggins interaction parameter has only been restricted and focused to a description of the enthalpy. It should also be stated in fitting the theory to real-life experimental data, it is found that that entropic effects have an impact on this parameter as well. There has been an effort to integrate entropic contributions to the Flory Huggins χ parameter [11]. As result, there is a more general expression of the Flory Huggins interaction parameter which has two terms:

$$\chi = \frac{A(\varphi)}{T} + B(\varphi) \tag{1.24}$$

The structure of the system, which is an input to estimate the entropy, affects the free energy of mixing, and this is described by the second term of the previous expression, whereas the first one refers to the dependence of the free energy to enthalpy.

Computationally, in our work, the Flory - Huggins interaction parameter is estimated by employing the Molecular Dynamics (MD) simulation method. This method allows us to estimate $\Delta_{mix}H$, v^*, V, φ_i at given T and use the equation 1.19 in order to estimate the χ value. A last comment at this point is that the entropic part has been ignored in this work. Future plans include the estimation of the entropic part by using Kirkwood-Buff theory.

Experimentally, there are many methods that can be employed to estimate the Flory - Huggins interaction parameter. The most important of them are: light scattering data [43], osmotic pressures [45], secondary ion mass spectrometry, atomic force microscopy and neutron reflectrometry [47]. One common drawback of these experimental techniques is that their results usually demonstrate significant discordance.

1.5 Phase Diagram

The global parameters governing the phase behavior of the BCPs in terms of thermodynamics are three: The Flory Huggins interaction parameter, the degree of polymerization, N, and the volume fractions which are expressed in equations 1.9 and 1.21.

Common periodic phases for diblocks, with increasing φ_1 include bodycentered cubic A spheres in a B matrix, hexagonally packed A cylinders in a B matrix, bicontinuous gyroid, and lamellae [9]. These phases are shown in figure 1.6. It should also be stated that there are some additional phases which are experimentally observed, but are not thermodynamically stable.

These thermodynamically stable structures on a nanometer-length scale that are shown on figure 1.6 are guided by the minimization of the free energy during the microphase separation. Block copolymer synthesis can easily determine whether microphase separation takes place, as well as the structure that is adopted, just by adjusting the degree of polymerization N and the volume fractions φ_i. The impact of the Flory Huggins χ parameter and the degree of polymerization N, can be clearly explained by interpreting the figure 1.7.

At this figure, L stands for lamellar phase separation, H stands for hexagonal

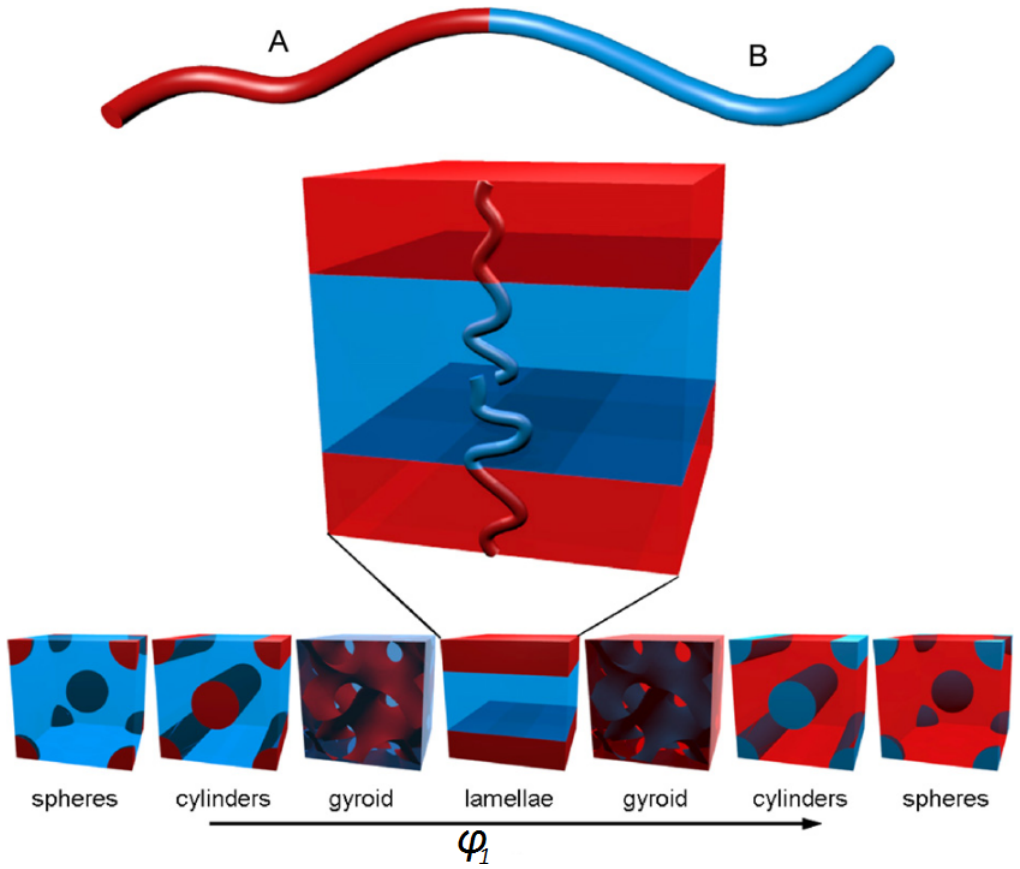

Figure 1.6: Schematics of thermodynamically stable diblock copolymer phases. [9]

cylinders, Qla3d stands for bicontinuous cubic gyroid, Qlm3m stands for BCC spheres and CPS stands for close-packed spheres. There is also a region at the bottom of the graph with DIS indication which stands for the disorder phase, where no phase separation takes place and the polymers are completely miscible. It is also clear that high values of χ and N lead to a strong degree of phase separation which is desirable in lithography applications and will be discussed in detail at the next chapter.

It should also be stated that figure 1.7 provides a theoretical and quantitative description of the phase separation, but it is efficient on qualitetivley demonstrating whether the segregation of the polymer domains is weak or strong. It is obvious that when the product of χ and N satisfies the equation $\chi N \leq 10.5$ (weak segregation limit) then no actual phase separation takes place. On the other hand, when $\chi N \geq 10.5$ is satisfied (strong segregation limit) then microphase separation and strong self assembled formations take place. All the above discussion is the outcome of the self consistent field theory and is made to describe the impor-

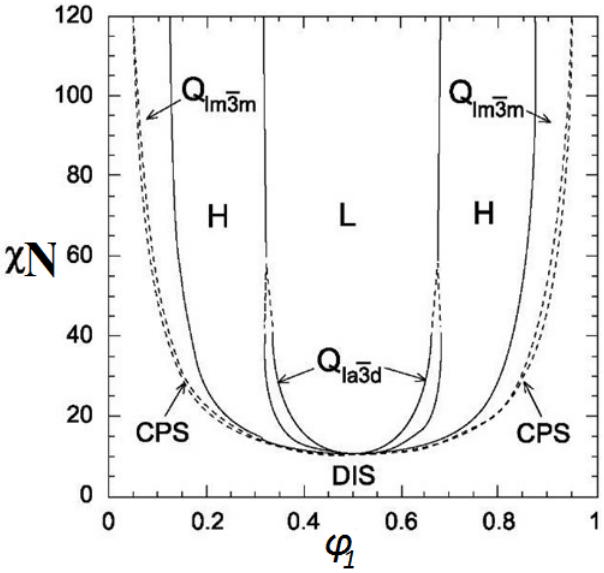

Figure 1.7: Phase diagram for model block copolymers. [36]

tance of χ in the resolution, which is only controlled by the degree of polymerization N and χ.

CHAPTER 2

Directed Self Assembly

2.1 Introduction

The purpose of this work is the computational study of the PDMS/PLA Polymer system, and the estimation of the Flory -Huggins interaction parameter χ. As discussed in the previous Chapter, this parameter describes the ability of the system to self-assemble and to form microdomains. This ability is highly desirable in the field of nanotechnology, especially in lithographic processes which are used for the fabrication of integrated circuits and patterns in the micro and nanoscale. Therefore, this chapter describes the lithography processes and the problems that modern industries have to cope with as the size scale of device features becomes ever smaller. Self Assembly and Directed Self Assembly of Block Copolymers are shown to provide an avenue for overcoming the challenges of diving into smaller dimensions and this is the reason why they are discussed in this chapter. Finally, there is also a description of the experimental techniques that are used to direct the self assembly of block copolymers for lithographic applications.

2.2 Lithography

Lithography has been the most important technology in manufacturing of integrated circuits and microchips and has revolutionized the semiconductor industry. It is a key technology that is used to create patterns whose size ranges from a few nanometers to micrometers and it is considered to be a traditional "top-down" method.

All the different lithography techniques can be categorized into to two types, according to the use of a mask [12]: masked lithography and maskless lithography. Masked lithography makes use of masks or even molds to create patterns over a large area. This category comprises photolithography, soft lithography, nanoimprint lithography and XUV lithography. On the other hand, maskless lithography techniques are the electron beam lithography, the focused ion beam lithography, and the scanning probe lithography. The most widespread of the above techniques, is photolithography (also known as UV lithograhy). Due to its importance to this work it will be described below.

A single photolithography procedure includes some steps. The first and probably the most important step is the thin film's (usually SiO_2) surface preparation, where typical contaminants must be removed. These contaminants severely affect the outcome of the process and could be dust, lint, bacteria, and photoresist residue from previous photolithography. The next step includes the photoresist application where the wafer is covered with photoresist by spin coating. The photoresist could be negative or positive, the main differences between the two categories being mainly three: The negative photoresist becomes insoluble after the exposure, whereas the positive becomes soluble (this may also be described in the literature as photosolubilization). In the case of the positive photoresist, the exposed parts become dissolved while in the case of the negative, the un-exposed parts become dissolved. The process that uses a negative photoresist is cheaper but offers poor resolution. After the photoresist application, the mask is precisely aligned to the wafer, and the exposure to UV light takes place. After the exposure to radiation, the unpolymerized photoresist is removed; this step is called development. Then the etching procedure takes pace, where a liquid chemical agent removes the uppermost layer of the substrate in the areas that are not protected by photoresist and finally the photoresist is removed. The whole procedure is shown in figure 2.1.

In general, patterns with features greater than 300 nm are usually produced by photolithography techniques. For pattern sizes between 300 and 30 nm, electron beam lithography is one of the most widely used experimental approaches. However, standard semiconductor lithography techniques are not efficient when it comes to pattern sizes less than 30 nm. Photolithography will likely never be abandoned by the semiconductor and data storage industries, but there is a crucial need to "dive" into smaller dimensions. Conventional photolithography encounters serious challenges when it comes to continuous miniaturization of IC in order to follow Moore's law and to deliver functional nanodevices into ever

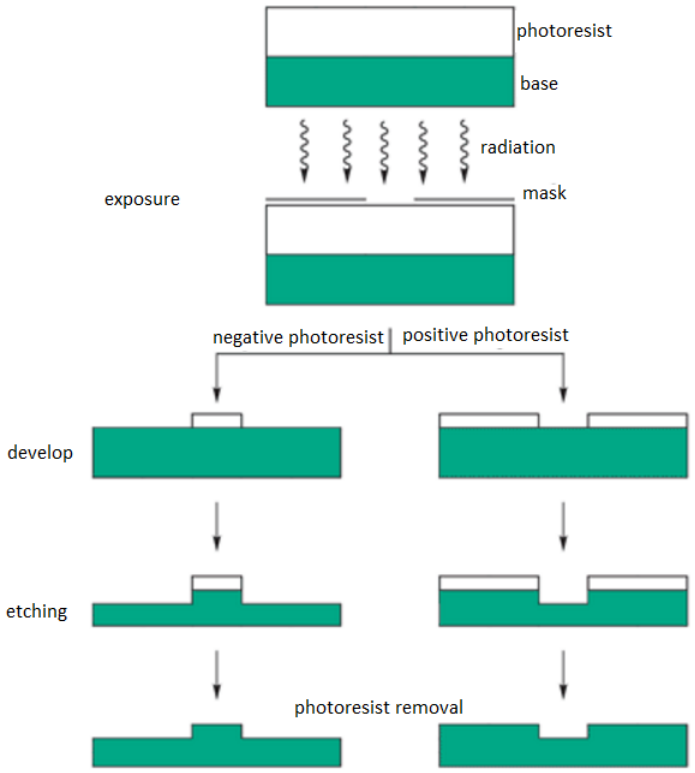

Figure 2.1: Photolithography Procedure . The resist material is applied as a thin coating, typically by spin coating over the substrate and heated to remove the solvent. The resist film is subsequently exposed in an image-wise fashion through a mask. The exposed resist film is then developed typically by immersion in a developer solvent to generate three-dimensional relief images.

smaller scales. A potential answer to that urgent need of miniaturization could be given by the Directed Self Assembly of BCs. This technique probably consists the most appropriate candidate for enhancing and guiding the resolution scaling of optical lithography. Due to its importance to this work, it will be described below.

2.3 Self Assembly

It would be an oversight not to describe what Self - Assembly is. Self-assembly can be defined as the autonomous organization of components into patterns or structures without human intervention [7]. Self-assembling processes are recurrently employed by nature and technology and mainly describe the appearance of order from disorder. The concept of these processes has been extensively stud-

ied during the past years and can be applied from the molecular to the planetary scale.

Given their fundamental importance and technological utility, materials that have the ability to self-assemble have been seriously considered for applications into a variety of disciplines such as drug discovery [21] and biology [22]. Another discipline that self-assemble processes can be applied, is nanotechnology. Inexpensive functional nanomaterials and devices have an increased impact and are extensively used in this field. At the nanoscale, Self Assembly can be described as a process by which nanoparticles or other discrete components spontaneously organize into ordered structures. This ability to form structures offers new perspectives to enhance and to develop new nanotechnology applications, because it permits scaling to the atomic scale. In the case of optical lithography though, many improvements could be made by directing the self assembly of block copolymers, a novel technique which will probably assist efforts to decrease the scale of essential geometries for integrated circuits (figure 2.2).

2.4 Directed Self Assembly

There is a distinction between Self-Assembly and Directed Self-Assembly (DSA). The act of directing implies a form of an "external" control over the self-assembly that is not present at the simple self-assembly process. The methods that are deployed for directing the self assembly proccedure will be discussed below. There is a definition for DSA, proposed by Eric M. Furst [24] : The term "directed" describes self-assembly in the presence of an externally applied field that introduces or modifies the interactions between constituents, leading to structures and phases that would not otherwise form in its absence. It may also refer to a process that uses an external means, typically flows or fields, to “nudge” the system into a desired (and presumably equilibrium) state.

This equilibrium state is governed by thermodynamic laws, as described in the first chapter. Free energy minimization drives the whole process and generates symmetric patterns. Conventional lithographic processes that have been used in the past decades become extremely difficult, and prohibitively expensive when the size scale of integrated circuits continuously becomes smaller. In particular, fabrication of integrated circuits and devices that have a feature size less than 45nm is almost impossible by optolithographic processes. Moore applications and miniaturization of integrated circuits can be extended and enhanced by employing the Directed Self-Assembly of block copolymers.

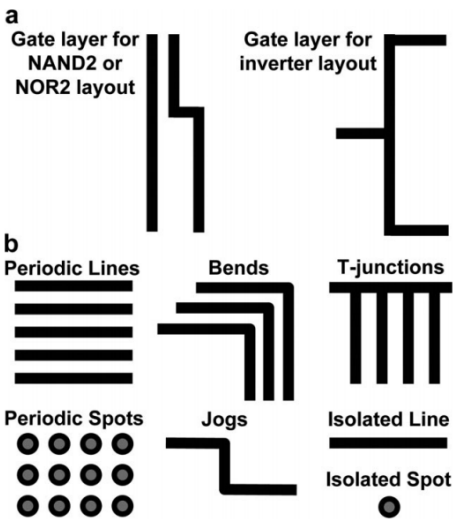

Figure 2.2: Essential geometries for integrated circuits [17]. The generalized layouts of the gate layer for some of the most basic circuit components, such as those for NAND2, NOR2, and inverter operations, require relatively simple pattern geometries. (b) The essential set of geometries required for fabricating most integrated circuits, as defined by the Semiconductor Industry Association's member companies, includes dense and isolated lines, dense and isolated spots, 90^o bends, jogs, and T-junctions.

BCs that are used for DSA purposes are mostly the diblock copolymers, that is, they only consist of two different polymers that are covalently bonded. The self organization of the A and B blocks via microphase separation is caused by the fact that they are thermodynamically incompatible. During this state of separation, the contacts between similar and dissimilar blocks are maximized and minimized, respectively. Put differently, connectivity constraints and the incompatibility between the blocks lead the block copolymers to self-assemble into nanometer-sized domains that exhibit ordered morphologies at equilibrium [9]. BCs are expected to merge the"top-down" traditional lithographic approach with the "bottom-up".

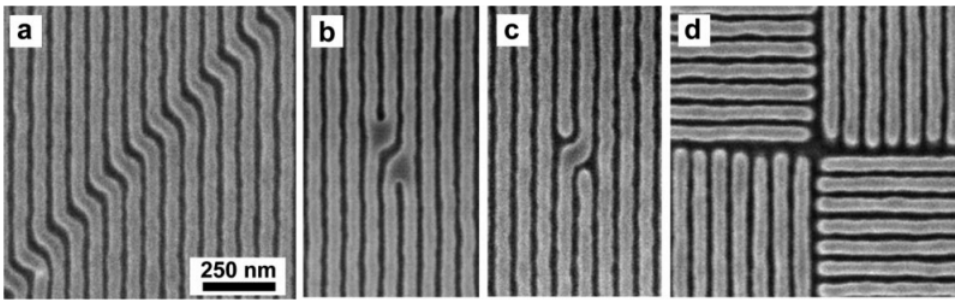

Figure 2.3: SEM images of the PS/PMMA BC directed to self assemble [17]. Top-down SEM images of the PS/PMMA ternary blend directed to assemble into (a) nested arrays of jogs, (b) isolated PMMA jogs, (c) isolated PS jogs, and (d) arrays of T-junctions. In all the SEM images, the PS domains are displayed in light gray, while the PMMA domains are dark gray or black.

The ability of BCs to self assemble gives the opportunity to use them as high resolution patterning materials for defining IC elements. The two major directing experimental methods to accomplish self assembly in block copolymers are chemical epitaxy and graphoepitaxy. Both methods relay on prepatterned substrates and enhance feature downscaling by multiplying spatial frequency on the prepattern. These methods are discussed below.

2.4.1 Graphoepitaxy

In the graphoepitaxy method, topographical features of lithographically prepatterned substrates are used to direct the self assembly. Block copolymer microphase separation takes place between predefined surface structures. Surfaces that consist of lithographically predefined topography, force block copopolymer thin films to form self-assembled morphologies whose orientation is guided along the topographic pattern directions. This method provides subdivision of the larger prepatterned lithographic units into sublithographic units, thus the lithography resolution is enhanced [39].

This method initially includes the formation of topographic structures into the resist or etching substrate material using conventional photolithography or electron beam lithography. This predefined template usually consists of SiO_2 and the BCs thin films are applied to its surface and guided with respect to the surface's orientation. By altering template shapes and block copolymer thickness, various structures can be obtained. After the deposition of the thin films over the substrate a spin coating process takes place and high temperature annealing is

employed. The prepatterned substrate is generally a physical confinement which forces the self assembly of the block copolymer domains, along the pattern edge. After the assembly, the nanodomains of one polymer are selectively removed and the nanodomains of the remained polymer are disposed to retain ordered functional nanopatterns[26]. The whole process of the graphoepitaxy method is shown in figure 2.4.

The graphoepitaxy method is mostly used to create cylinder arrays (figure 2.5) and lamellar formations. As a relatively new experimental method, has its own drawbacks and needs to be improved. In detail, non-uniform thickness of the over coating polymer thin films and imperfect predefined topographical patterns deteriorate the placement accuracy and the microphase separation process.

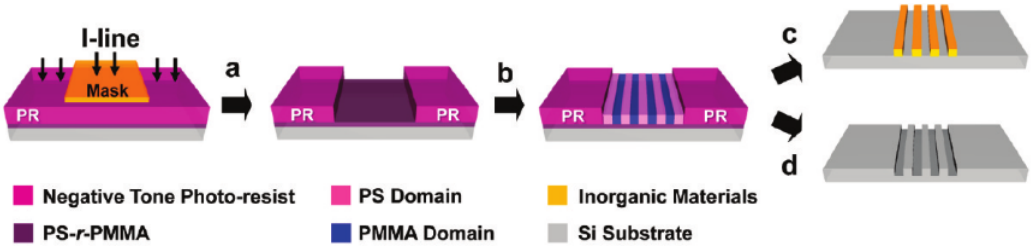

Figure 2.4: Representation of the graphoepitaxy process for PS-b-PMMA BCs [26]. a .Patterning of negative tone photoresist by a projection photolithography. b. Spin coating of PS-b-PMMA and thermal annealing for directing the self assembly c. and d. selected removment of PMMA nanodomains and pattern transfer by selective deposition or selective etching.

2.4.2 Chemical Epitaxy

In the chemical epitaxy method, lithographically-prepared dense chemical patterns dominate the self assembly process. These patterns consist of chemically controlled spatial variations. The precise placement of the block copolymer domains is guided by the chemical affinity between the chemical patterns at the substrate and the block copolymer domains.

The prepared substrate is a lithographically defined chemically heterogeneous surface, consisting of alternating pinning stripes of width W_P and chemically and thermodynamically neutral stripes of width W_N. Evidently, the pitch of the sparse chemical patterns (P_S) is larger than the pitch of the block copolymer assembly (P_{BCP}) and satisfies the expression [38]:

$$P_S = W_N + W_P \tag{2.1}$$

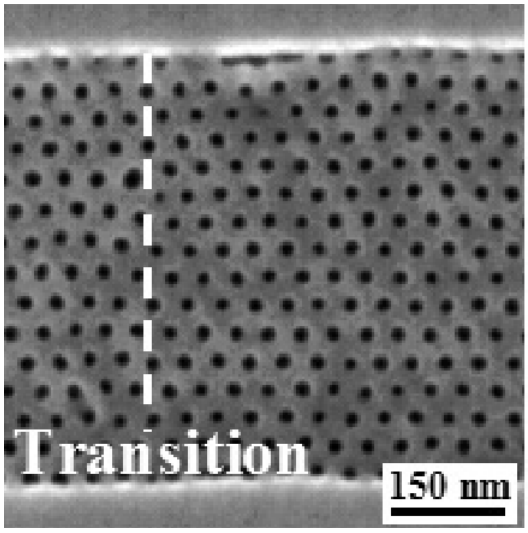

Figure 2.5: Coexistence of 13 and 14 rows of PMMA cylinders produced by graphoepitaxy in a groove with a 536 nm width and cylinder dimeter d=22nm. [40]

The pinning stripe has higher chemical affinity for one block, so a particular polymer domain is located on the pinning stripe, whereas the neutral stripes are similarly affinitive to both blockd omains. This process leads to the creation of perpendicularly oriented block copolymer domains. Frequency multiplication is controlled by the factor of P_S/P_{BCP}. The final step of the chemoepitaxy method includes selective removal of a domain of the block copolymer, usually by oxygen reactive ion etch or plasma etch. The removed domains are replaced by spaces in the resultant line-space pattern after etch [38, 41]. The whole process is shown in figure 2.6.

It should be underscored that the chemistry of the prepatterned surface is a key feature for a successful DSA procedure. However, this experimental method needs to be improved since there are some drawbacks. At first, the prepatterned surface is vulnerable to imaging processes, as in the case of electron beam radiation, so prior imaging may affect or block the DSA process. For that reason, the materials that comprise the chemical prepattern are usually removed along with the block copolymer during the etching. Another drawback of the chemical epitaxy is that it is a prohibitevly expensive method, when it comes to massive production. This happens due to the fact that the fabrication of the chemical prepatterns is made by electron beam or extreme ultraviolet lithography, which are known to have an increased cost [38].

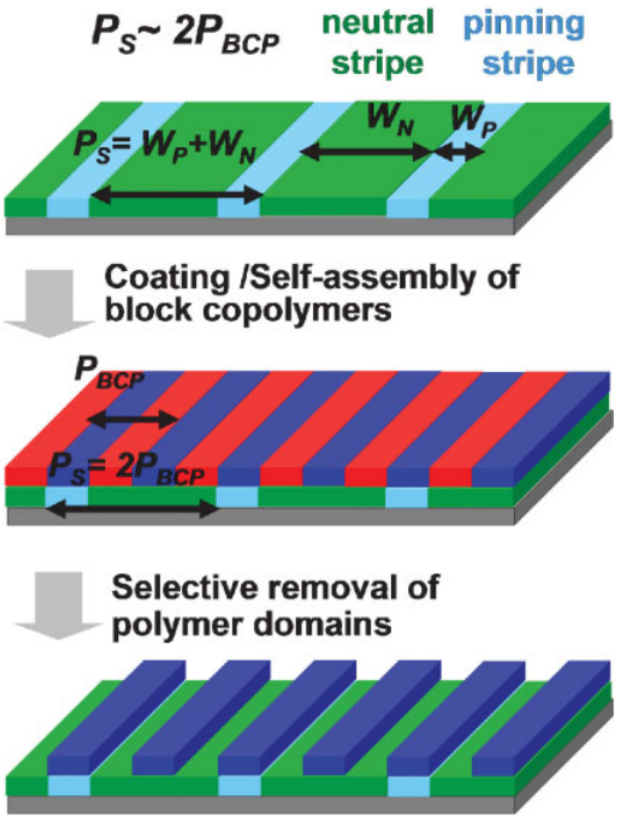

Figure 2.6: Chemical epitaxy steps [38]. Preparation of a substrate that has pinning stripes which demonstrate higher chemical affinity for one block. Then the coating takes place where the block copolymers self assemble. Finally, a selective removal of a specific polymer domain takes place. .

CHAPTER 3

Systems Studied

3.1 Introduction

Probably the most used block copolymer in block copolymer lithography that has also been experimentally studied a lot, is Poly(styren)-b-Poly(methyl methacrilate). This block copolymer offers a positive interaction parameter χ around 0.04, that is it constitutes a good candidate for DSA applications. However, in order to enhance and improve DSA applications, there is a need to find and deliver new block copolymers that exhibit higher χ values. In other words, tailoring and using materials that have the ability to efficiently self-assemble in smaller feature sizes will give the opportunity to "follow" Moore Law and to diminish dimensions for nanotechnology and lithography purposes. Silicones (polymers that include any inert, synthetic compound made up of repeating units of siloxane) usually demonstrate significantly high χ values when they are copolymerized with other polymers, thus, they are of great interest for the semiconductor industry. The materials that have been computationally studied in this work include two poly-mers, Poly (dimethylsiloxane) and Poly (lactic Acid), as well as their blend. Poly (dimethysiloxane) is a silicone, so it is supposed to critically contribute to a high χ value of the material. The unique properties and applications of these materials are separately discussed below.

3.2 Poly(dimethyl siloxane)

Polydimethylsiloxane (PDMS - Πολυδιμεθυλοσιλοξάνιο) is a physically and chemically stable, silicon-based elastomer with a potential and wide range of applications. It is a mineral-organic polymer (a structure containing carbon and silicon) of the siloxane family (a word derived from silicon, oxygen and alkane). The PDMS empirical formula is $(C_2H_6OSi)_n$, n being the degree of polymerization.

Its structure is unique and can be characterized as semi-organic, with a polar inorganic backbone Si - O. The bond between the Si and O is long and strong (bond energy 445 kJ/mol) and the angle of Si - O - Si is wide open. These bonds enable to obtain a flexible polymer chain with a high level of viscoelasticity, flexibility and large free volume. Its structure also includes nonpolar organic methyl substituents. The bond between the Si and the methyl substituents is short and the intermolecular forces are weak, a common characteristic in elastomers. As a result, PDMS is a very chemically stable material known for its thermal stability and it is also able to resist aging, moisture and ultraviolet radiation. As for its surface activity, having a low surface tension (20.4mN/m), it can easily wet many surfaces. Plus, its methyl groups align in the most favorable position leading to a water repellency behaviour making it hydrophobic.

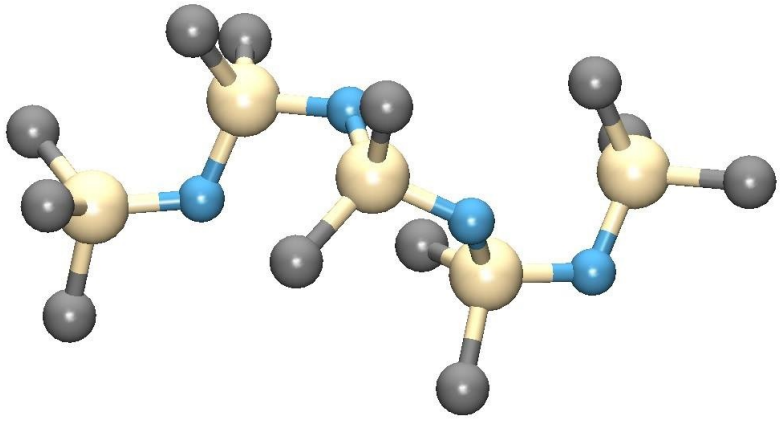

Figure 3.1: United Atom PDMS pentamer structure

Compared to other polymers, PDMS has a unique attribute and that is its extremely low glass transition temperature ($T_g = -125^oC$). As in most polymers, the glass transition temperature depends on the molecular weight, but this will be discussed on Chapter 3. Silicones, like PDMS, also experience high oxygen and nitrogen permeability. The structure of a PDMS pentamer is shown in figure

3.1.

As stated above, PDMS is used into a wide range of applications. It can be embedded in electronic components, which prolongs the lifespan of the chip. Thereby, PDMS acts as a dielectric isolator and protects the components from environmental factors and mechanical shock within a large temperature range (at least from -100^oC to 100^{o}C) [27]. In addition, PDMS is a very popular silicone elastomers used in the fabrication of microfluidic devices in numerous lab-on-a-chip (LOC) applications [28]. Moreover, it is not toxic for cells and its gas permeability and water impermeability make PDMS suitable for a variety of biological and microfluidic applications [37].

3.3 Poly(lactic acid)

Polylactic Acid (PLA - Πολυγαλακτικό οξύ) is one of the most promising biopolymers (polymers used for biological purposes) and can be produced by a large number of techniques.

PLA belongs to the family of aliphatic polyesters. These polyesters are commonly made from α hydroxyl acids, which also includes polyglycolic acid (PGA), polycaprolactone and polydioxanone. PLA is a copolymer that can be obtained by the polymarization of LLA and DLA enantiomers. That is, it is one of the few polymers that has a stereochemical structure that can be easily modified by polymerizing a controlled mixture of L and D isomers to yield a high-molecular-weight and amorphous or semicrystalline polymer. What should be underscored is that the ratio of D to L enantiomers affects many important properties of PLA. Both D and L enantiomers are shown in figure 3.2. A structural representation of a PLA pentamer is shown in figure 3.3. Its glass transition temperature is around 335K [42] and as in the case of PDMS and other polymers, it depends on the molecular weight.

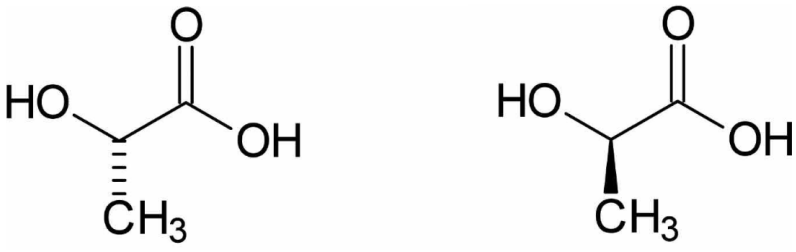

Figure 3.2: D (left) and L (right) enantiomers.

Polymers that are used for thermoplastic applications have properties such as thermal stability and impact resistance, that are in general superior to those of PLA. In contrast, PLA is one of the most promising and extensively used biodegradable materials. That is, it eliminates the need to remove implants and provides long term biocompatibility. In other words, PLA is a polymer that can adapt well to a biological environment without causing adverse effects on tissues. PLA has also been used in various forming processes, such as injection moulding, extrusion moulding and foaming, and so on.

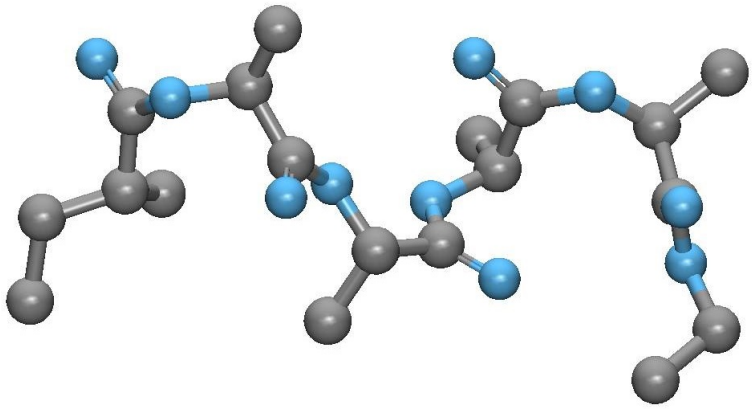

Figure 3.3: United Atom representation of a PLA pentamer.

3.4 PDMS/PLA Blend

The widespread usage of PS - PMMA block copolymer derives from the fact that it may form well defined morphologies at the micro scale, so it is suitable for DSA applications. However this system has its own drawbacks. The χ parameter may be positive (that is, the two domains are immiscible) but it is still relatively low. For that reason, high molecular weights are required to achieve microphase separation. In order to provide solutions to the problem, Fe and Si containing groups such as poly(hedral oligomeric silsequioxane) (POSS) and PDMS have been seriously considered for block copolymer lithography. Block copolymers that contain the groups mentioned above can achieve microphase separation more easily since the χ parameter that describes their immiscibility is higher.

Apart from the higher χ parameter offered by Fe and Si containing groups, as in PDMS-b-PLA which is studied in this work, there is also another reason why these groups have attracted attention. Jung and Ross [18] stated in their work

that ideal BCs, apart from high χ value, should also include a domain which demonstrates high etch selectivity . These selectively etchable domains allow the pattern to be precisely formed into the material. The Si in the PDMS offers high etch resistance to O_2 RIE, but it can also be selectively etched in the presence of PLA by fluorinated etchants. Being both eatch resistant and susceptible,it offers the possibility to form both dot and antidot arrays [29]. In this work we simulated the PDMS/PLA blend in order to estimate the χ parameter between PDMS and PLA. The outcome of the simulation will be used to study PDMS-b-PLA.

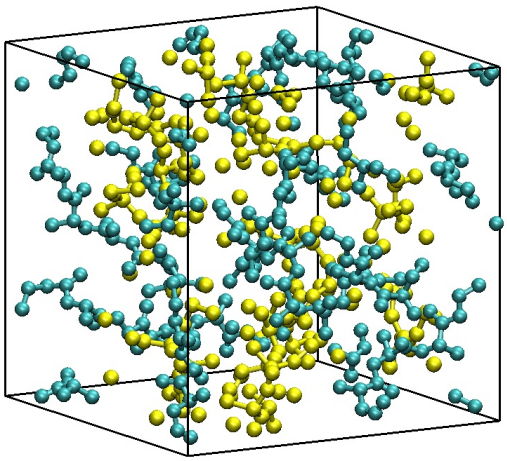

Figure 3.4: Simulation box of PDMS/PLA Blend, generated by MAPS software

On the other hand, high χ materials generally need more energy to self-assemble, thus a longer process time is required. Consequently, it is very important to identify the best compromise between resolution and processing time. This would facilitate the selection of the right material. Rodwogin et in stated at their work that dimensions of 3nm could be achieved by the used of PDMS-PLA-PDMS triblock copolymers, thus the PDMS-PLA copolymer constitutes one of the most suitable candidates for DSA applications.

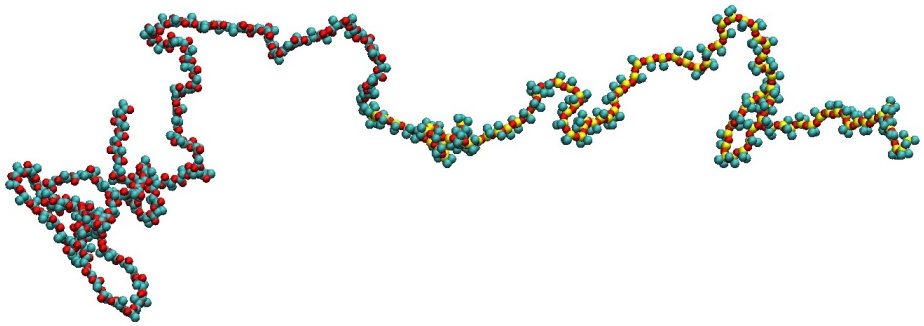

Figure 3.5: PDMS - PLA Block Copolymer structure, generated by MAPS software

CHAPTER 4

Atomistic Simulations

4.1 Introduction

Materials modelling and simulations constitute a very important discipline that has greatly benefited from the advance of computer technology. Complex computational methods that were impossible to apply due to computer time limitations, have nowadays become an indispensable part of materials science and engineering, providing an alternative and efficient way of tackling problems related to modern industrial demands. Material properties can be computationally studied and predicted, thus the design of novel materials with a potential of applications is significantly enhanced. As stated in previous chapters, one of the most important factors affecting the self assembly process is the χ interaction parameter. Atomistic simulations are able to guide the selection of high χ materials and estimate properties that are directly related to block copolymer lithography. In this work, two different methods have been used: Molecular Dynamics (MD) and Monte Carlo Simulations (MC). MD is a determinstc method, that is the configuration of the system at any future or past time can be computed from its current configuration. MC is a stochastic method and randomly generates configurations by using a special set of criteria. Both of these methods are separately discussed below.

4.2 Molecular Dynamics

Molecular Dynamics (MD) is a method that describes the "real" dynamics of the system, allowing the user to calculate time averages of properties. The main concept of this method is that Newton's equations of motion are applied to derive sets of atomic positions. As a result, MD is a deterministic method, that is the future and the past of each state of a system can be predicted from its current state. Newton's laws of motion are applied to the initial configuration of the system and generate future configurations. As a result, positions and velocities of a system are specified by a trajectory which is obtained by the following differential equation, embodied in Newton's second Law:

$$\frac{\partial^2 \vec{r}_i}{\partial t^2} = \frac{\vec{F}_i}{m_i} \tag{4.1}$$

The previous equation describes the motion of a particle of mass m_i along coordinates $\vec{r}_i$ with $\vec{F}_i$ being the force that causes the motion. In order to perform MD simulations, there is a need of an appropriate force field that would be used as an input to the Newton's laws. A description of the force fields is given at the end of this chapter. The force fields provide a useful expression for the total potential energy $\mathcal{V}_i$ of the system. This is used by Newton's second law as follows:

$$\vec{F}_i = -\vec{\nabla}_{\mathbf{r}_i} \mathcal{V}_i \tag{4.2}$$

Integration of the equations of motion is usually made by the widely used Verlet algorithm. The Verlet algorithm uses the positions and accelerations at time t, and the positions from the previous step, $\vec{r}(t-\delta t)$, to calculate the new positions $\vec{r}(t+\delta t)$. We may write the following expressions for $\vec{r}(t+\delta t)$ and $\vec{r}(t-\delta\tau)$:

$$\begin{aligned} \vec{r}(t+\delta t) &= \vec{r}(t) + \delta t \vec{v}(t) + \frac{1}{2}\delta t^2 \vec{a}(t) + ... \\ \vec{r}(t-\delta t) &= \vec{r}(t) - \delta t \vec{v}(t) + \frac{1}{2}\delta t^2 \vec{a}(t) + ... \end{aligned} \tag{4.3}$$

It shoud be noted that $a(t)$ is obtained as $\frac{\vec{F}(t)}{m}$ Adding the previous equations we obtain:

$$\vec{r}(t+\delta t) = 2\vec{r}(t) - \vec{r}(t-\delta t) + \delta t^2 \vec{a}(t) \tag{4.4}$$

The velocities $\vec{v}$, can be estimated from the previous expressions:

$$\vec{v}(t) = \frac{\vec{r}(t+\delta t) - \vec{r}(t-\delta t)}{2\delta t} \tag{4.5}$$

All the previous discussion included the factor δt which describes the time step we use to integrate. With a very small time step, the system progresses through phase space very slowly, leading to time consuming simulations. A very large time step, on the other hand gives instabilities.

In order to run an MD simulation, we need to specify the initial atomic coordinates and velocities. Classical mechanics is deterministic, that is, the initial state with the interaction potential specify the entire future and the entire past. In this work we have used the MAPS software [35] developed by Scienomics SARL in order to do so. The numerical integration, as described above, is a deterministic algorithm. This is important because the simulation must be reproducible. On the other hand, in order to obtain statistically meaningful results, for systems with long correlation times it is advantageous to run a bunch of different simulations from different initial conditions rather than running just a single lone trajectory starting from a single initial state.

Sometimes, balance problems that may create a huge total energy of the system are caused by innapropriate initial configurations. In these cases, energy minimization of the system prior to MD is highly recommended. The energy minimization takes apart atoms that were extremely nearby, in the initial configuration. The minimization procedure is driven by the derivative of the free energy with respect to each independent variable. In this work, we have used the open-source LAMMPS software to run MD simulations. This software invokes the conjugate gradient method [1] to do energy minimization [15, 48]. All MD simulations conducted on NPT ensemble of constant pressure (1atm) and temperature.

4.3 Monte Carlo Simulations

The Monte Carlo (MC) method is one of the most widely used methods for statistical sampling purposes and was firstly applied to a class of stochastic numerical problems by scientists working at the Los Alamos National Laboratory, in order to develop nuclear weapons [48]. This method was the first to be used for molecular modelling purposes. Its main difference from other computational

[1] At each iteration the force gradient is combined with the previous iteration information to compute a new search direction perpendicular (conjugate) to the previous search direction. The Polak–Ribière (PR) variant affects how the direction is chosen and how the CG method is restarted when it ceases to make progress. The PR variant is thought to be the most effective CG choice for most problems.

methods arises from the fact that it is a stochastic method due to the use of random numbers. The main concept of this method for material purposes, is the simulation of a thermodynamic system that changes its thermodynamic states, until it reaches a final state of thermodynamical equilibrium.

In Monte Carlo simulations, thermodynamic properties are estimated by a stochastic sampling of great number of configurations of a system. The sampling process of these configurations is governed by the probability density that is imposed by the macroscopic conditions on the system. For instance, consider an MC simulation of N molecules at temperature T in a box of volume V. Each configuration m is sampled by the grand canonical statistical ensemble density of probability:

$$P_m^{NVT} = \frac{e^{-\beta \mathcal{V}_m}}{\sum_{\text{all states}} e^{-\beta \mathcal{V}_m}} \tag{4.6}$$

where $\mathcal{V}_m$ is the potential energy of configuration m and $\beta = \frac{1}{k_B T}$, where k_B is Boltzmann's constant. A move is attempted in each step of a MC simulation which usually changes the position or the orientation of a specific part of the system that is studied, leading to a new configuration. The probability α_{mn} of attempting to go to a new configuration n from the configuration m usually satisfies the expression:

$$\alpha_{mn} = \alpha_{nm} \tag{4.7}$$

In many cases, as in the case of this work, simulations that do not satisfy the previous expression are sometimes more useful. The probability of accepting the new configuration is $\min(1, \frac{p_n \alpha_{nm}}{p_m \alpha_{mn}})$ where p_n is the a priori bility of n. As a result, the conditional probability p_{nm} of adopting the configuration n given the configuration m is:

$$p_{nm} = \alpha_{nm} \min\left(1, \frac{p_n}{p_m}\frac{\alpha_{nm}}{\alpha_{mn}}\right) = \begin{cases} \alpha_{mn} & p_n \alpha_{nm} \geq p_m \alpha_{mn}, \quad m \neq n \\ \frac{p_n}{p_m}\alpha_{nm} & p_n \alpha_{nm} < p_m \alpha_{mn}, \quad m \neq n \end{cases}$$

Apparently:

$$p_{nm} = 1 - \sum_{m \neq n} p_{mn} \tag{4.9}$$

In the case of $\alpha_{mn} = \alpha_{nm}$, the criterion of acceptance above is known as Metropolis selection criterion [16].

There are different ways of employing the Monte Carlo method, in order to study a system. Despite their plethora, all the methods have a similar process.

Polymer melts and systems in general, demonstrate significant complexity and thus can not be easily studied in total. This happens because many materials have complex chemical structure (especially when they contain side branches), are governed by extremely slow system dynamics (as in the case of Poly(methyl methacrylate)) and might also have coulomb interactions, making the system extremely difficult and time-consuming for employing Monte Carlo simulations. Regardless of the complexity, the structure of a polymer chain affects many of its most important properties. For all the reasons above, instead of performing Monte Carlo simulations for polymer melts, we employ the single chain Monte Carlo simulation method. This method is quite useful for estimating some important conformational properties, such as the charateristic ratio (stiffness) and Kuhn's Length.

In single chain Monte Carlo methods we simulate unperturbed polymer chains that only exhibit local interactions. The term "local interactions" is used to indicate bonded interactions and nonbonded interactios active between sites that are relatively close along the contour of a chain. Intermolecular interactions diminish the contribution of the intramolecular ones. As a result, the monomers of a single chain are not likely to interact with other monomers of the same chain, especially when they are not relatively close. In order to mimic this behaviour of a polymer system, in single chain Monte Carlo simulations only local interactions of an unperturbed chain are considered.

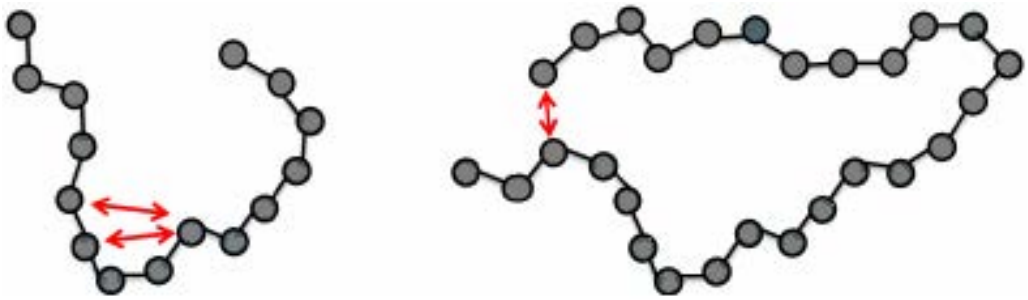

Figure 4.1: Local (left) and non- local interactions (right).

One could request more information regarding which monomers are considered to be relatively close along the chain or what are the intramolecular interactions that are described by the term local. The answer to this question is given by one parameter that is used as an input from the user, in order to perform single chain Monte Carlo simulations, and that is Δn_{pair}. Van der Waals and Coulomb interactions are the intramolecular local interactions that affect the total energy of

the chain. Instead of considering all monomers in order to calculate these local interactions for a single monomer, a specific number of "neighbouring" monomers is taken into account, and this number is defined as the Δn_{pair} parameter. In other words this number is the maximum allowed distance between groups between which pairwise calculations take place. The higher the value of this parameter, the more local interactions are used as an input to estimate the total energy of the chain. If Δn_{pair} number is high, then the chain will collapse to itself [5] . That is, too many Lennard Jones interactions are considered thus the attractive forces become dominant and the chain takes a globule conformation. On the other hand, if Δn_{pair} number is low, then the intramolecular interactions can not be used efficiently as an input to the energy of the system. In order to estimate the most appropriate value for Δn_{pair} we use an empirical rule, namely that the optimal value of Δn_{pair} is the one that produces the highest value of stiffness. A reluctant reader could say that the rule described above is empirical, so it lacks of scientific integrity. For that reason, a validation with multi chain Monte Carlo simulations usually takes place. The Δn_{pair} parameter, for a a part of PDMS chain is demonstrated in figure 4.2.

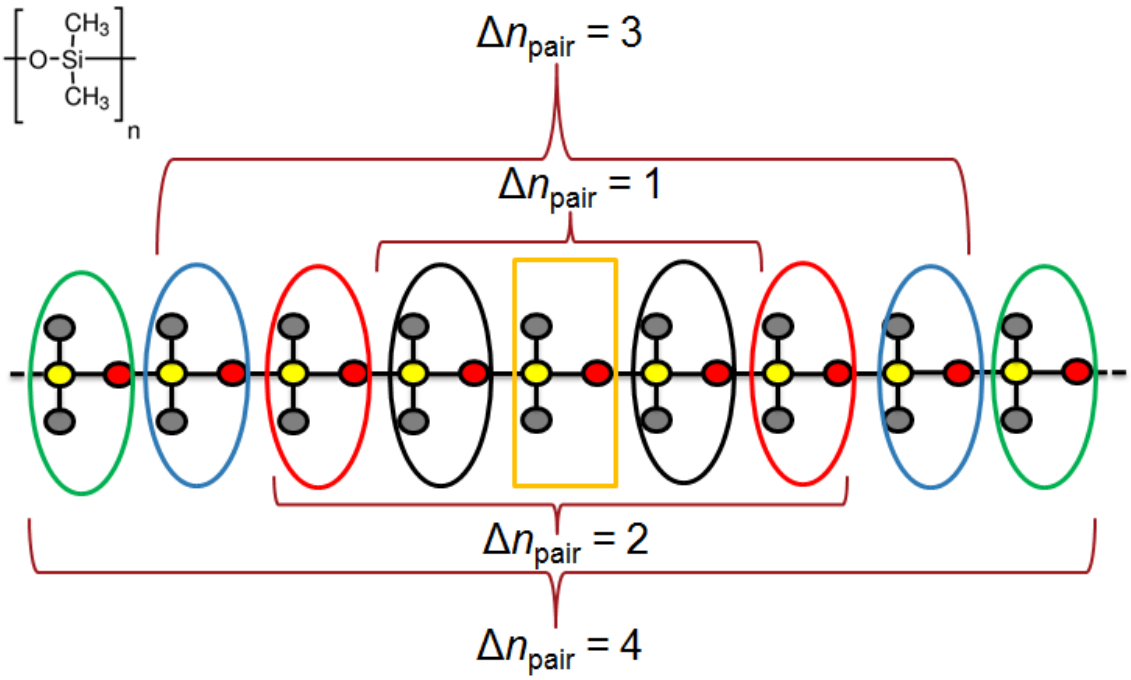

Figure 4.2: Δn_{pair} demonstration for a PDMS chain. Red circles represent the oxygen atoms, yellow circles represent the silicon groups and gray circles represent the methyl groups (CH_3)

It would be beneficial at this point to describe the single chain Monte Carlo procedure. At first, an initial configuration of a single polymer chain is generated. We have used the MAPS software in order to do so. Lets consider the system's initial energy:

$$\mathcal{V} = E_{bond} + E_{angle} + E_{dihedral} + E_{imp} + E_{LJ} + E_{coul} \tag{4.10}$$

The second step includes a Monte Carlo move where one of the five available moves is picked. These moves will be described later. After a selected move the energy of the system becomes:

$$\mathcal{V}^{'} = E^{'}_{bond} + E^{'}_{angle} + E^{'}_{dihedral} + E^{'}_{imp} + E^{'}_{LJ} + E^{'}_{coul} \tag{4.11}$$

And the difference between the initial and the final energy apparently is:

$$\Delta\mathcal{V} = \mathcal{V} - \mathcal{V}^{'} \tag{4.12}$$

Then we use Metropolis acceptance criteria in order to determine whether we will accept the new move or not:

$$\begin{gathered} \Delta\mathcal{V} < 0 \\ \text{or} \\ \Delta\mathcal{V} > 0 \quad \text{and} \quad \xi < e^{-\frac{\Delta\mathcal{V}}{k_B T}} \end{gathered} \tag{4.13}$$

Where ξ is a random number, k_B is the Boltzman's constant and T is the temperature. In the case of accepting the new move, the system configuration is changed and we proceed to another iteration step. In the case of not rejecting the move, another iteration step takes place without changing the system's configuration. The whole Monte Carlo procedure is shown in Figure 4.3.

Finally, before closing the description of the Monte Carlo method, we should describe the moves that are used to make the simulation. There are five different moves. The first is a single atom displacement move and refers to the backbone atoms of the polymer chain. Initially a united atom along the backbone is selected randomly. A cubic box in created around the atom and the atom is allowed to move inside that cubic box. The second move is the flip atom move where an atom along the backbone is selected and a random angle ω is chosen in order to rotate it around the axis connecting the atoms on either side of the moved atom. At this move no bond lengths change and apparently the total bond energy remains the same. The above moves are shown in figures 4.4 and 4.5.

The third move is the rotate strand move (Pivot). An atom is selected randomly as well as a chain strand to rotate with a rotation angle φ. Again no bond

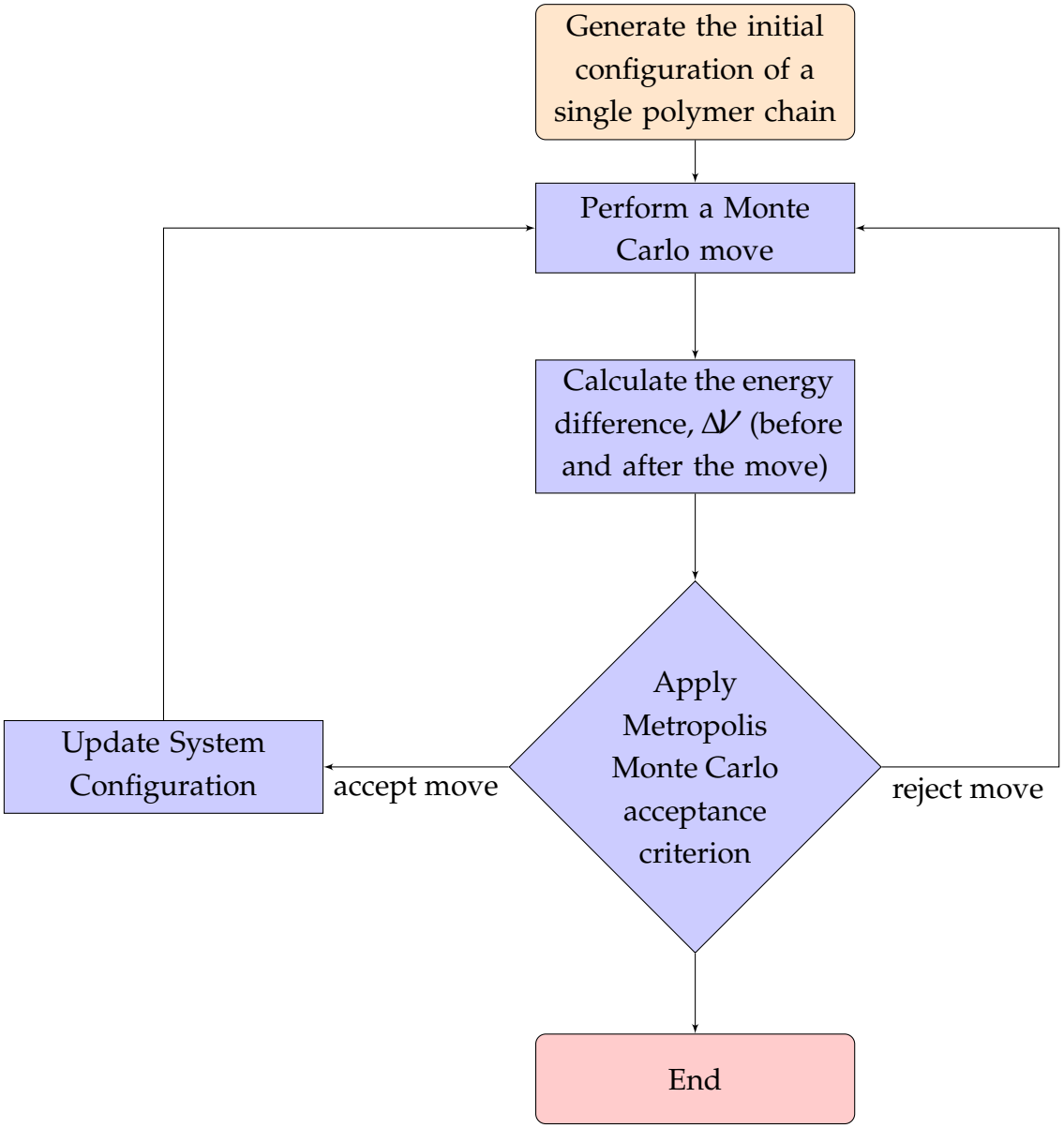

Figure 4.3: Monte Carlo Flow Process. An initial configuration of a single polymer chain is generated. The second step includes one of the five Monte Carlo moves and then the difference in energy before and after the move is calculated in order to apply the Metropolis Monte Carlo acceptance criterion.

lengths or bond angles change and the total bond and angle energy remain the same. This move is shown in figure 4.6.

Finally, the two last moves refer to the polymer branch. The first move is the flip branch move. A branch is selected randomly and is flipped around the axis by a randomly selected angle φ. As in the previous moves, no bond lengths

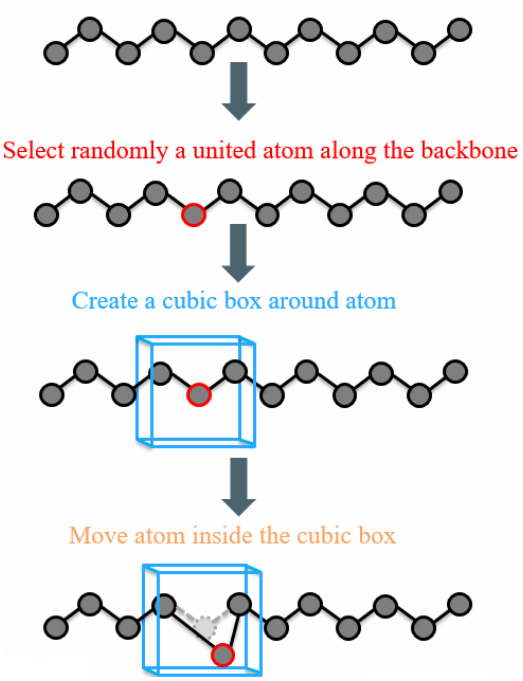

Figure 4.4: Single atom displacement move. A united atom is selected randomly. A cubic box in created around the atom and the atom is allowed to move inside that cubic box.

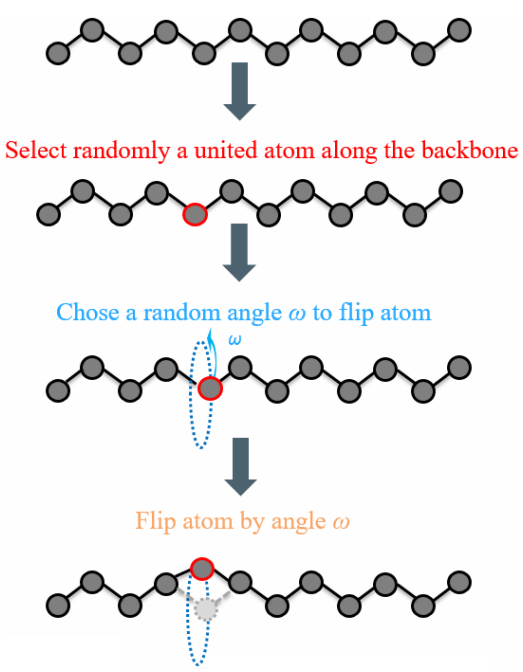

Figure 4.5: Flip Atom Move. an atom along the backbone is selected and a random angle ω is chosen in order to flip the atom. At this move the bond lengths do not change.

change and the total bond energy remains the same. The final move is the rotate branch where a branch is again selected randomly and rotated by a randomly selected angle φ. As in the previous branch move, no bond lengths change and the total bond energy remains the same.

4.4 Force Fields

Intra- and inter- molecular forces within a system that is studied are the key factor to run a successful simulation. All of these forces should be embodied in a force field $\mathcal{V}$ that consists of two contributions, a bonded and a non-bonded one, as demonstrated in the following equation:

$$\mathcal{V}(\vec{r}^N) = \mathcal{V}_{\text{bonded}} + \mathcal{V}_{\text{non bonded}} \tag{4.14}$$

At the previous equation, $\vec{r}^N$ is the vector of each atom, and the total number of atoms is defined by N. Bond length deviations and rotations and bond angle deviations from their reference values, lead to energetic penalties, which are

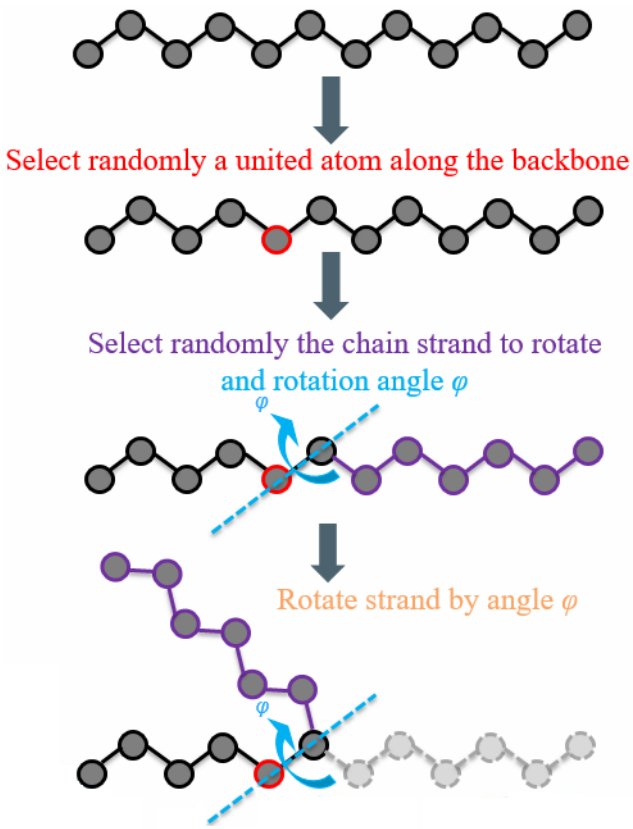

Figure 4.6: Rotate Strand Move (Pivot). An atom is selected randomly as well as a chain strand to rotate with a rotation angle φ.

embodied in the first term of the previous expression. This is of the following general form:

$$\mathcal{V}_{\text{bonded}} = \sum_{\text{bonds}} \frac{1}{2} k_i (l_i - l_{i,0})^2 + \sum_{\text{angles}} \frac{1}{2} d_i (\theta_i - \theta_{i,0})^2 + \sum_{\text{torsions}} \sum_{n=1,5} A_n \cos^{n-1}(\varphi) \tag{4.15}$$

From the previous expression we observe that bond and bond angle potentials have the same Hooke's law formula in which the energy varies with the square of the deviation from the reference value $l_{i,0}$ for bonds and $\theta_{i,0}$ for angles. The third term, also known as torsional, refers to rotation around bonds and its for is obtained by LAMMPS.

The second term of equation 4.14 refers to the non bonded interactions and usually is given by the following expression:

$$\mathcal{V}_{\text{non bonded}} = \sum_{i=1}^{N} \sum_{j=i+1}^{N} 4\varepsilon_{ij} \left(\left(\frac{\sigma_{ij}}{r_{ij}} \right)^{12} - \left(\frac{\sigma_{ij}}{r_{ij}} \right)^{6} \right) + \sum_{i=1}^{N} \sum_{j=i+1}^{N} \frac{q_i q_j}{4\pi\varepsilon_0 r_{ij}} \tag{4.16}$$

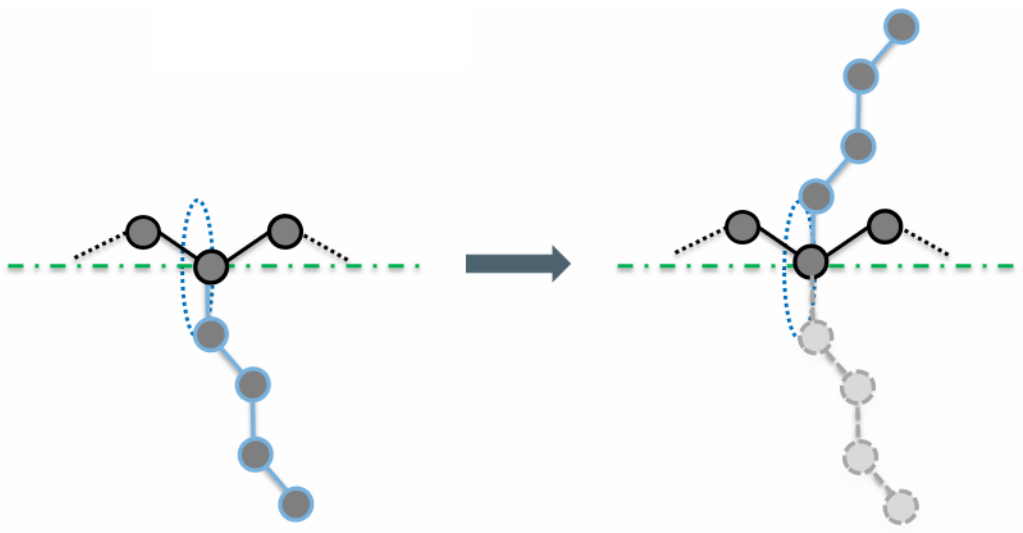

Figure 4.7: Flip Branch Move. A branch is selected randomly and is flipped around the axis by a randomly selected angle φ.

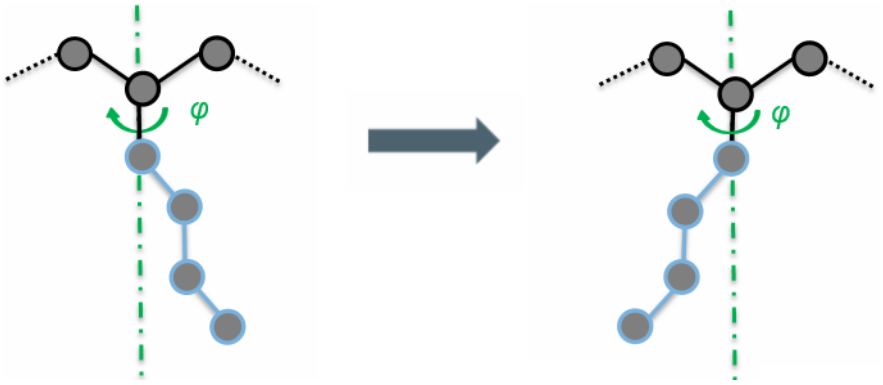

Figure 4.8: Rotate Branch Move. Aa branch is again selected randomly and rotated by a randomly selected angle φ.

The previous expression refers to pairs of atoms (i and j). The first term refers to a Lennard-Jones potential, which encompasses a steeply repulsive and a more gradual attractive term with a well and describes the interaction between pairs of molecules i and j. $\varepsilon_{i,j}$ is the depth of the potential well, σ_{ij} is the finite distance at which the inter-molecular potential is zero and r_{ij} is the distance between the particles. Instead of a 12-6 LJ potential we may also have a 9-6 form. The second term of the previous expression refers to Coulomb interactions between molecules of charges q_i and q_j. These interactions are estimated using Ewald summation. $\sigma_{i,j}$

and $\varepsilon_{i,j}$ are estimated using the Lorentz-Berthelot rules:

$$\begin{aligned} \sigma_{ij} &= \frac{\sigma_i + \sigma_j}{2} \\ \varepsilon_{ij} &= \sqrt{\varepsilon_i \varepsilon_j} \end{aligned} \tag{4.17}$$

For PLA, we used a TraPPE - United Atom force field and the parameters were taken from papers [30, 31, 32]. For PDMS we also used a TraPPE-UA force field developed by Curro et al [33]. It this paper, Si and O were treated differently and different mixing rules than the regular Lorentz-Berthelot were proposed. For the depth of the LJ potential ε_{ij} between O and Si containing groups, they proposed the following expression:

$$\varepsilon_{ij} = \frac{2\sigma_i^3 \sigma_j^3 \sqrt{\varepsilon_i \varepsilon_j}}{\sigma_i^6 + \sigma_j^6} \tag{4.18}$$

and $\sigma_{i,j}$ is given by the expression:

$$\sigma_{ij} = \left(\frac{\sigma_i^6 + \sigma_j^6}{2} \right)^{1/6} \tag{4.19}$$

The LJ potentials between Si and O containing groups have the form:

$$\mathcal{V}_{ij}(r) = \varepsilon_{ij} \left(2\left(\frac{\sigma_{ij}}{r_{ij}}\right)^9 - 3\left(\frac{\sigma_{ij}}{r_{ij}}\right)^6 \right) \tag{4.20}$$

In the Appendix, we list the LJ parameters used at this work for PDMS, PLA and PDMS/PLA blend as well as information regarding the partial charges, helping the reader to reproduce results and to repeat simulations.

CHAPTER 5

Results and Discussion

5.1 Introduction

In parallel with experimental measurements, many material properties can nowadays be studied and predicted by simulations. Simulations and computational methods in general have become an indispensable part of modern materials science and engineering due to the fact that they provide an alternative and often a less costly and time-consuming avenue of studying and predicting the properties of new materials. This relatively new discipline is also employed to guide the production of new materials as well as the selection of others in order to justify whether they are suitable for specific purposes and applications. Volumetric, dynamical, solubility and conformational properties are of significant importance and can be studied computationally. In the case of DSA, apart from the aforementioned properties, the Flory-Huggins interaction parameter as well as the enthalpy of mixing constitute a crucial criterion in order to examine whether specific materials are suitable. The block copolymer of PDMS-b-PLA is one of the most promising candidates for block copolymer lithography, since it may offer formations at the scale of 3nm [29], providing a way of efficiently reducing dimensions.

5.2 Volumetric Properties

The volumetric properties that have been studied in this work are the density and isothermal compressibility. Both properties are discussed below for both

polymers.

5.2.1 Density

The density is commonly defined as the quotient of mass per volume, and is given by the following simple expression:

$$\rho = \frac{nM}{< V >_{NpT}} \tag{5.1}$$

Where n is the number of moles and M is the relative formula mass. Computationally, the density can easily be estimated by dividing the mass of the simulation system by its volume. In order to explore the impact of the temperature on the density, we performed four MD simulations of pentamer systems at 400K, 450K, 500K and 550K. The results for PDMS and PLA are shown in figures 5.1 and 5.2. Available experimental densities of PDMS and PLA were obtained from [8] and from [44] respectively. The experimental values for PDMS are available for short chains while for PLA refer to the long chain regime.

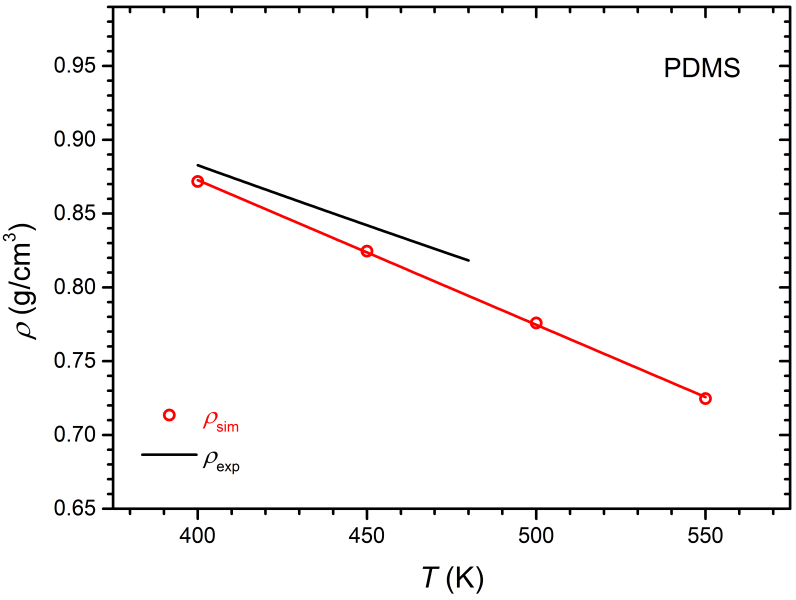

Figure 5.1: Density of PDMS. Black line corresponds to experimental measurements and is obtained from [8]. We performed four MD simulations at 400K, 450K, 500K and 550K and the values of density that we obtained are shown with the red dots. We then used the least squares method in order to find a linear curve that fits the simulation dots.

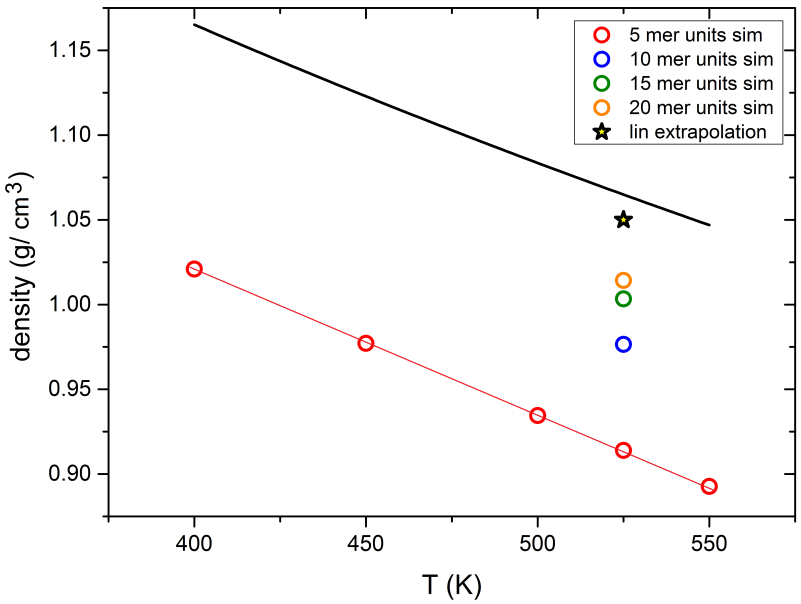

Figure 5.2: Density of PLA. Black line corresponds to experimental measurements and is obtained from paper [44]. We performed four MD simulations at 400K, 450K, 500K, 525K and 550K and the values of density that we obtained are shown with the red dots. We then used the least squares method in order to find a linear curve that fits the simulation dots. In order to get an estimate of the impact of the chain's length to the density we simulated chains consisting of 10, 15 and 20 mer units as well. We finally emplyed linear extrapollation in order to see how the experimental results can be described by simulations.

We observe a significant dependence for the density on the temperature. Thermal expansion takes place in both polymer melts, since the increase in temperature causes an increase of their volume. An experimental equation of density of PDMS was received from [8]. The complete formula of the experimental equation is:

$$\rho = 0.9919 - (8.925(T-273)10^{-4}) + (2.65(T-273)^2 10^{-7}) - (3(T-273)^3 10^{-11}) \tag{5.2}$$

The equation above is defined from 450K to 480K and refers to long PDMS chains. In the previous expression, density is given in $\frac{g}{cm^3}$ and temperature in K. This expression might have a complex form but it mainly exhibits a linear behaviour

as well as the curve that fits the simulation values: [1]

$$\rho = -10^{-4}9.8T + 1.265 \tag{5.3}$$

In the previous expression, density is given in $\frac{g}{cm^3}$ and temperature in K. For PLA, the experimental equation that describes the dependence of density on the temperature is found in [44] and it is the following:

$$\rho = \frac{1.1452}{1 + 0.00074(T - 423.15)} \tag{5.4}$$

The previous equation might also have a complex form but it mainly demonstrates a linear behaviour as well as the curve that fits the simulation values:

$$\rho = -10^{-4}8.54T + 1.36 \tag{5.5}$$

In PLA we observe that there is a discordance between simulation and experiment, due to the fact that simulations refer to polymer chains that only consist of five mer units, whereas the available experimental data refers to very long chains. For that reason we simulated chains that consist of ten, fifteen and twenty mer units. We also performed a linear extrapolation to see if the experimental results can be approached by the simulation ones. In order to do so, we plotted on the y axis the densities estimated for various chain lengths and on the x axis the fraction $\frac{1}{\text{mer units}}$. This plot is shown on figure 5.3.

We obtained the following equation:

$$y = 1.0532 - 0.76388x \tag{5.6}$$

Setting x as zero, we are able to estimate the value of density for very long chains. This value is included in figure 5.2. We observed that the chain's length has an impact in simulations as well and the linear extrapolation we performed estimates a value of density close to the experimental data.

In both polymers simulation and experimental estimations show a strong dependence on the temperature. The slope of the simulation curve in the case of PDMS is higher than the corresponding slope of PLA, thus a temperature increase leads to a higher density decrease in PDMS than in PLA. We should also state that in the case of PLA, the curve that fits the densities obtained by MD methods, is not consistent with the experimental one, and this is because we simulated PLA pentamers, while the experimental results refer to PLA macromolecules. For that reason, we also performed MD simulations for longer chains.

[1] In order to estimate the equation that fits the experimental dots, we used the famous least squares method.

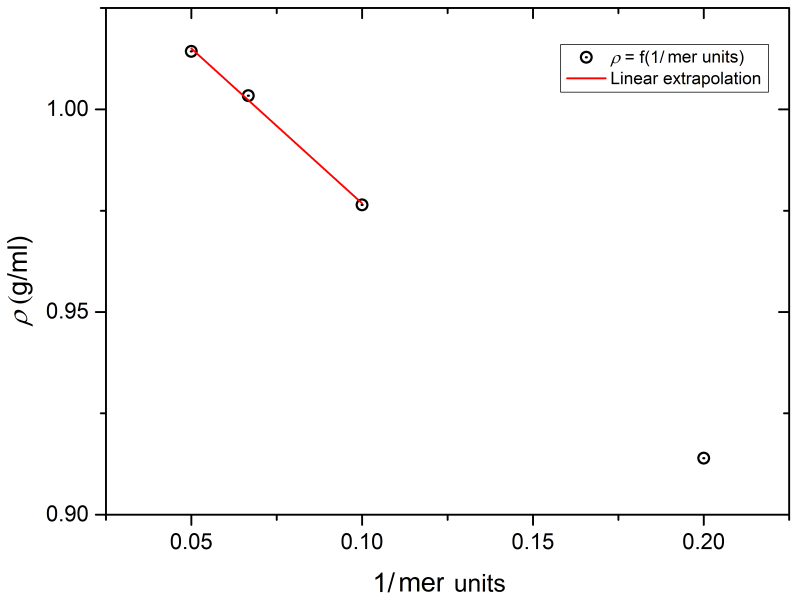

Figure 5.3: Linear Extrapolation of PLA.

5.2.2 Isothermal Compressibility

At constant temperature, the extent to which the volume of a fluid changes with pressure is quantified by the isothermal compressibility β_T. Its definition is given below:

$$\beta_T = -\frac{1}{V}\left(\frac{\partial V}{\partial P}\right)_T \tag{5.7}$$

An easily compressible polymer has a large value of β_T. In order to estimate the isothermal compressibility we performed MD simulations because they provide the values of volume fluctuations during the simulation procedure. As a result, by using the following expression we were able to estimate β_T [49]:

$$\beta_T = \frac{< V^2 > - < V >^2}{k_B T < V >} \tag{5.8}$$

We may notice from the previous expression that the isothermal compressibility is related to the mean square volume displacement. Figures 5.4 and 5.5 show the simulation results for PDMS and PLA. Experimental results for PDMS are also presented.

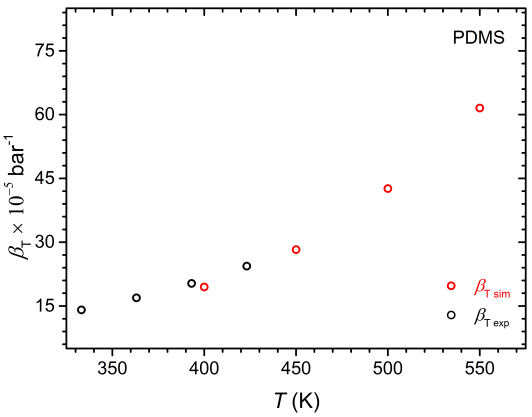

Figure 5.4: Simulation and experimental results for isothermal compressibility for PDMS [57].

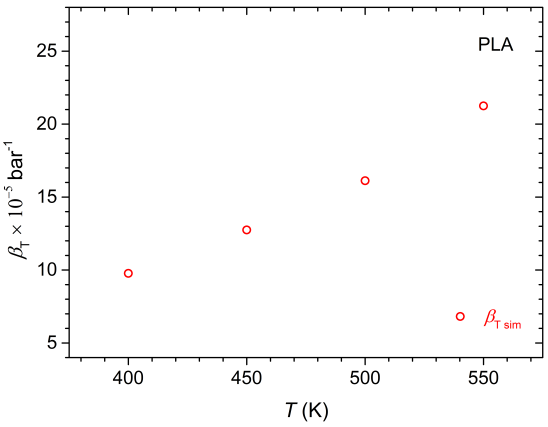

Figure 5.5: Simulation and experimental results of isothermal compressibility for PLA.

There is a significant agreement between the computed isothermal compressibilities and the experimental ones in the case PDMS. Unfortunately no experimental results were found in the literature for PLA.

5.3 Characteristic Ratio (Stiffness)

The characteristic ratio is a conformational property. Initially, the stiffness should be defined. Bond angles and torsional potentials have a great impact on the flexibility of the polymer chains that constitute polymer melts. The End to End vector $\overrightarrow{R}$ is defined as the vector that connects thefirst united atom of the backbone of the chain, with the last, as is it demonstrated in figure 5.6. The mean square end to end distance of very long chains is given by the expression:

$$< \overrightarrow{R}^2 >= C_n n l^2 \tag{5.9}$$

where n is the number of backbone bonds, l is the bond length and C_n is Flory's characteristic ratio. The characteristic ratio is larger than unity ($C_n > 1$) for all polymers and reflects the conformational stiffness of the chain. In other words, the higher value of C_n the stiffer the polymer chains are. There is also a tendency for polymers that have bulky side branches to exhibit large values of C_n i.e., be stiffer. The characteristic ratio also increases increasing chain length and reaches a plateau value C_∞ for very long chains. This plateau value is characteristic for each polymer and reflects its conformational distribution. The dependence of the

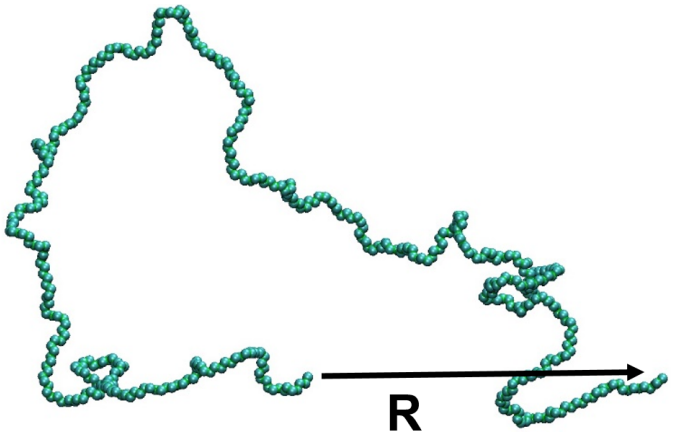

Figure 5.6: End to End Vector.

Flory's characteristic ratio on the chain length is qualitatively demonstrated in figure 5.7.

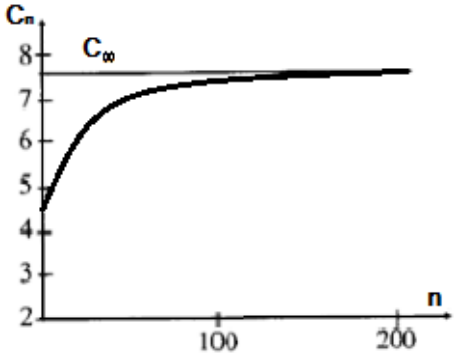

Figure 5.7: The depence of Flory's Characteristic Ratio on the Polymer length [34]. C_n reaches a plateu value C_∞ for long chains.

Experimentally, the characteristic ratio is usually estimated by two different methods and these are the Small - Angle Neutron Scattering (SANS) and intrinsic viscosity measurements. Computationally, the characteristic ratio is estimated by application of the Rotational Isomeric State model [15]. In this work, the characteristic ratio is estimated by single chain Monte Carlo method which has been described in chapter 5. The results for PDMS are shown in figure 5.8.

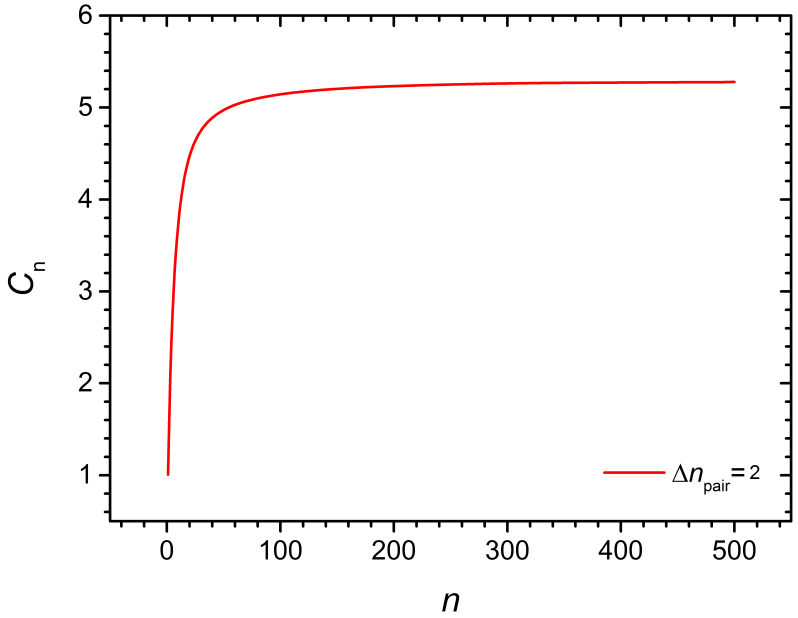

Figure 5.8: Characteristic ratio for PDMS. The Δn_{pair} number that is used to estimate the caracteristic ratio is 2.

The characteristic ratio for PDMS is estimated as 5.68. Both experimental and simulation results are shown in the table below:

Monte Carlo Simulation	Experimental	Temperature (K)
5.38	6.25 [50]	298

Table 5.1: PDMS characteristic ratio: experimental and simulation results at 450K.

The simulation results for PLA are shown in figure 5.9.

Simulation and experimental results are different but not significantly different. The results for PLA are shown in the table above:

Monte Carlo Simulation	Experimental	Temperature (K)
6.1	6.7 [58]	413

Table 5.2: PLA characteristic ratio: experimental and simulation results.

In order to estimate the characteristic ratio for PDMS, the value of Δn_{pair} is 2; and above 3 the chain collapses. In the case of PLA, Δn_{pair} is 1 and the chain collapses when $\Delta n_{pair} > 3$. The simulation prediction is closer to experiment in the case of PLA. It is also obvious that PLA is stiffer than PDMS. The disparity

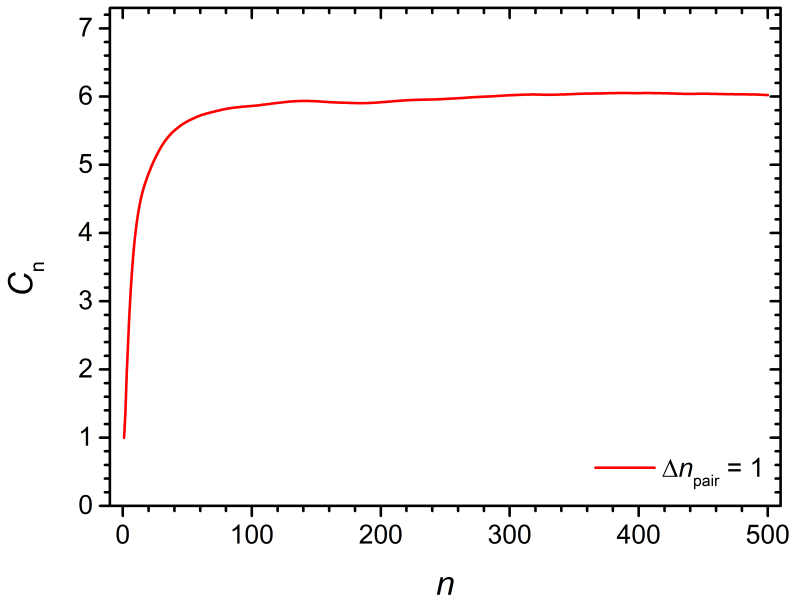

Figure 5.9: Characteristic ratio for PLA. The Δn_{pair} number that is used to estimate the caracteristic ratio is 1.

between experimental and simulated values is caused by the force field we used, since it seems that it fails to describe accurately the stiffness of the chains.

5.4 Dynamical Properties

In this work the dynamical properties that have been studied are the glass transition temperature, the longest relaxation time and the self diffusion coefficient. All these properties are separately discussed below.

5.4.1 Glass Transition Temperature

The glass transition is the reversible transition in amorphous materials and polymers (or in amorphous regions within semicrystalline materials) from a hard and "glassy" state into a molten and viscoelastic state, as the temperature is increased. The glass-transition temperature T_g of a material is the temperature over which this glass transition occurs.

In order to study the glass transition temperature for PDMS and PLA by molecular simulations, an analysis of the time autocorrelation functions of two different vectors was made. In the case of PDMS, the vector characterizing the orientation of the Si-O bond is of great importance, while in the case of PLA a

crucial role in the segmental dynamics is played by the bond vector of C-O. Let this vector be denoted as $\overrightarrow{v}$. The time dependence of the second Legendre polynomial term can be expressed by using the vectors $\overrightarrow{v}$:

$$P_2(t) = \frac{3 < \left(\overrightarrow{v}(t)\overrightarrow{v}(0)\right)^2 > -1}{2} \tag{5.10}$$

where the brackets <> are used to indicate the average of the autocorrelation function over all bond unit vectors, $\overrightarrow{v}$, along the chain for all chains of the system and $\overrightarrow{v}(0)$ represents the initial vector. The evolution of the vector $\overrightarrow{v}$ through time is tracked by MD simulations in the molten state and can be used in order to obtain the second Legendre polynomial. $P_2(t)$ is well described by a Kohlrausch-Williams-Watts (KWW) function [56]:

$$P_2(t) = a_l e^{-\frac{t}{\tau_l}} + (1 - a_l)e^{-(\frac{t}{t_k})^\beta} \tag{5.11}$$

The expression above encompasses two terms. The first describes a fast exponential decay with amplitude a_l. This amplitude is associated with the fluctuations and librations of torsion angles around backbone bonds and with the bond length fluctuations and bond angle bending vibrations of backbone and pendant bonds, with characteristic time τ_l. The second term is not as fast as the first and consists of a stretched exponential decay. It is associated with conformational transitions in the polymer chain. t_k is the characteristic correlation time of the chosen vector and β the stretching exponent. The smaller the value of β in comparison to 1, the more cooperative the dynamics. By using equation 5.10, we are able to perform a four parameter curve-fitting test on the MD results in order to estimate a_l, τ_l, t_k and β by using the Levenberg-Marquardt algorithm [2]. The second order Legendre polynomials for PDMS and PLA, are shown in figures 5.10 and 5.11 respectively for various temperatures.

MD simulations were made for different temperatures for the two polymers. In the case of PDMS simulations took place for temperatures at 200K, 220K, 240K, 260K, 280K and 300K, whereas in the case of PLA the temperatures were 400K, 410K, 425K, 450K, 475K, 500K, 525K and 550K. That difference emerged from

[2]The Levenberg–Marquardt algorithm (LM algorithm) is an iterative numerical method, used to solve non-linear least square problems. Given a set of k pairs (x_i,y_i), this algorithm tries to optimize the parameter vector $\overrightarrow{\beta}$ of the curve f(x, $\overrightarrow{\beta}$) in order to minimize the sum of squares of the deviation: $\sum_{i=1}^{k}[y_i - f(x_i, \overrightarrow{b})]^2$. In order to start the minimization, the user makes an initial guess of the β parameters b. After each iteration, the $\overrightarrow{\beta}$ parameters, are replaced by by a new estimate $\overrightarrow{\beta} + \overrightarrow{\delta}$, where $\overrightarrow{\delta}$ is given in the expression: $f(x_i, \overrightarrow{\beta} + \overrightarrow{\delta}) = f(x_i, \overrightarrow{\beta}) + J_i \overrightarrow{\delta}$ and $J_i = \frac{\partial f(x_i, \overrightarrow{\beta})}{\partial \overrightarrow{\beta}}$ is the gradient of $f(x_i, \overrightarrow{\beta})$ with respect to $\overrightarrow{\beta}$.

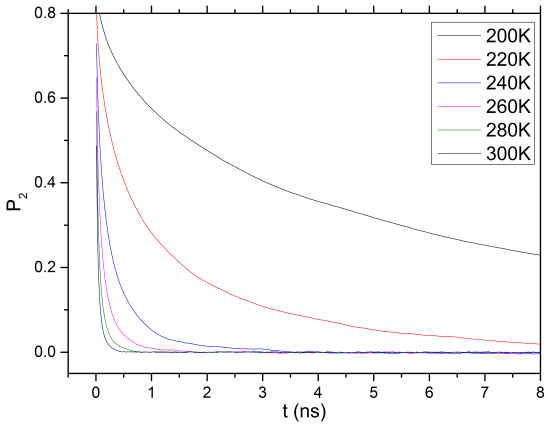

Figure 5.10: Second order Legendre Polynomial for PDMS at 200K, 220K, 240K, 260K, 280K, and 300K.

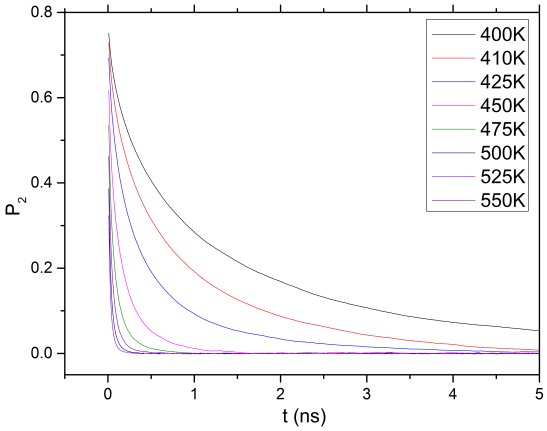

Figure 5.11: Second order Legendre Polynomial for PLA at 400K, 410K, 425K, 450K, 475K, 500K, 525K and 550K.

the fact that PDMS has a very low glass transition temperature in comparison with other polymers such as PLA, and in order to be able to computationally study the glass transition temperature we had to perform simulations at lower temperatures.

Having estimated these four parameters for PDMS and PLA at various temperatures, the segmental relaxation time t_c at each one of these temperatures can be given by the expression below:

$$t_c = \int_0^\infty P_k(t)dt = a_l\tau_l + (1 - a_l)t_k\frac{1}{\beta}\Gamma(\frac{1}{\beta}) \tag{5.12}$$

The estimated a_l, τ_l, t_s, β and t_c parameters for various temperatures are provided in tables A5 and A6 at the appendix. The well known formula of Williams-Landel-Fery (WLF) connects the segmental relaxation time t_c with the glass transition temperature T_g as follows:

$$\log\left(\frac{t_c}{t_g}\right) = -\frac{c_1(T - T_g)}{T - T_g + c_2} \tag{5.13}$$

In this formula, t_c and t_g are the correlation times at temperatures T and T_g respectively. The temperature dependence of the relaxation times for PDMS and PLA obtained from MD simulations, as well as the WLF fit according to equation 5.13 are shown in figures 5.12 and 5.13.

The parameters c_1, c_2, and T_g for PDMS and PLA that were obtained from the WLF curve fit, again by using the LM algorithm, are shown in table 5.3.

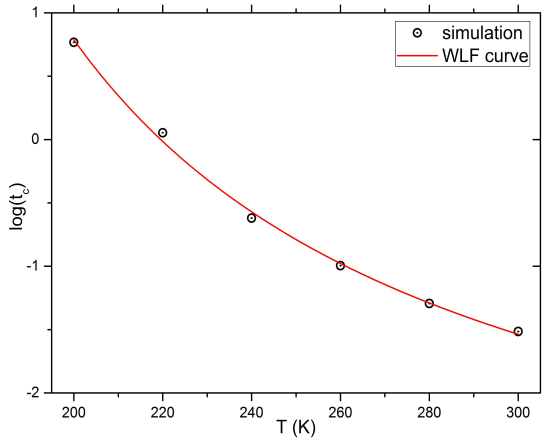

Figure 5.12: Temperature dependence of the relaxation times for PDMS obtained from from MD simulations through analysis of the $P_2(t)$ autocorrelation function of the bond's vector Si-O. Fits to the WLF equation are also presented, generated by the LM algorithm. t_c is given in ns.

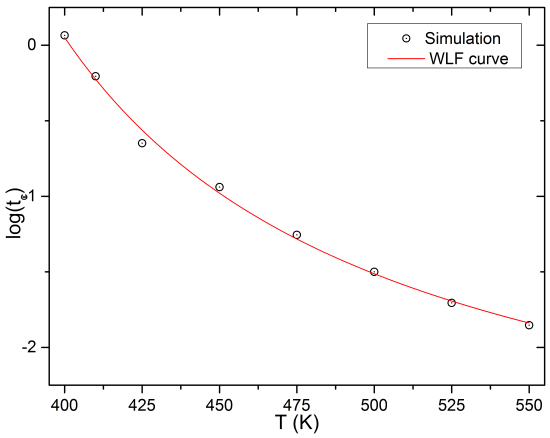

Figure 5.13: Temperature dependence of the relaxation times for PLA obtained from MD simulations through analysis of the $P_2(t)$ autocorrelation function of the bond's vector C-O. Fits to the WLF equation are also presented, generated by the LM algorithm. t_c is given in ns.

Table 5.3: Values of c_1, c_2, t_c and T_g of WLF equation four parameter test for PDMS and PLA. Glass transition temperature for PDMS was estimated as 131.7K and for PLA as 307.8K.

	PDMS	**PLA**
c_1	14.58	23.05
c_2/K	18.21	15.07
T_g (K)	131.7	307.8

The glass transition depends on the molecular weight (M_w) of each polymer and increases with increasing the molecular weight, but their relation is not linear. For very high molecular weights the glass transition does not change significantly as in the case of small and medium molecular weights. In order to examine how accurate were the simulation results of the glass transition, we should plot them with the experimental results that are given for different molecular weights. In figures and 5.14 and 5.15 the experimental and simulation results are plotted together for PDMS and PLA respectively.

We observe that the dependence of the glass transition on molecular weight is significant for small values of the molecular weights. The simulation results for the glass transition of PDMS and PLA are 131.6K and 307.8K respectively. Exper-

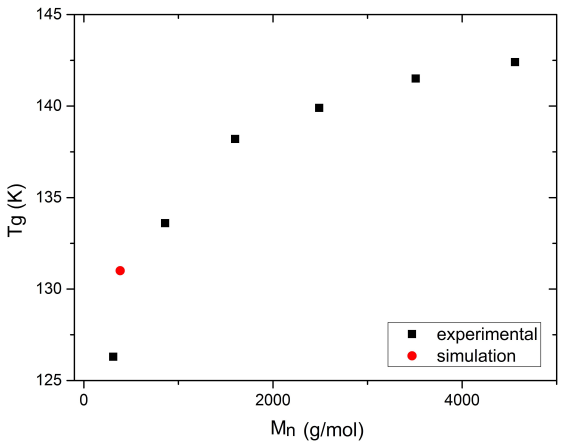

Figure 5.14: Experimental results against the simulation result for the glass temperature of PDMS. The simulation result is in great accordance with the experimentals, and follows the trend.

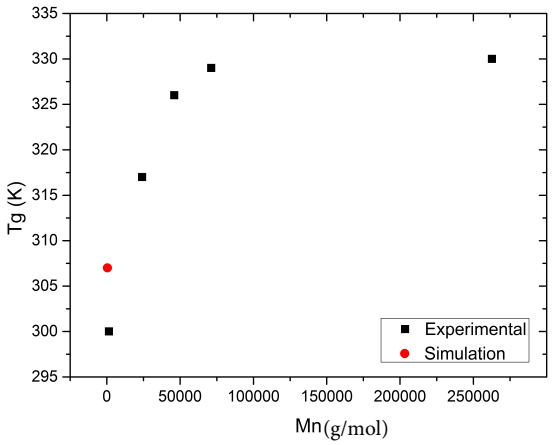

Figure 5.15: Experimental results against the simulation result for the glass temperature of PLA. The simulation result is in accordance with the experimental [53].

imental values of T_g for PDMS and PLA obtained from [54] and [53], respectively. In this work, as stated in chapter 3, we simulated PDMS and PLA pentamers of molecular weight 384.83 and 418.44 $\frac{g}{mol}$ respectively. Unfortunately, there were no expiremental results of the glass transition temperature for these exact molecular weights. In the case of PDMS we observe that the simulation result follows the trend of the increase of the glass transition temperature with increasing the molecular weight. This is a way of validating the forcefield we used, and we may safely say that it reproduces very well the dynamical properties of PDMS. In the case of PLA though, the simulation result of glass transition temperature should have a higher value, since the experimental value of T_g for a PLA chain of higher molecular weight (=1473) is lower (=300K), but we may say that there is no significant discordance. Another interesting thing to comment at this point, is that the WLF parameters (c_1 and c_2) for the PDMS are in great accordance with the experimental. Kirst et al [54] performed dielectric spectroscopy for linear and cyclic PDMS chains of various molecular weights and they estimated the c_1 and c_2 parameters. c_1 and c_2 for a PDMS that consists of 8 mer units were estimated 13.68 and 18.18 respectively. The values of WLF parameters that we estimated by a four-parameter curve fit of the WLF equation are 14.58 and 18.21K and they are very close to the experimental values. Unfortunately, no WLF parameters were found in the literature for PLA. Generally, the overall good agreement between the calculated and experimental PVT properties for PDMS and PLA is an indica-

tion of the force field's efficiency to describe the segmental dynamics of these two polymers.

5.4.2 Longest Relaxation Time

When the chains consist of a few monomer units and they are in the melt state, their conformational dynamics can be described by the Rouse Model. In this model, the chains are envisioned as consisting of spheres (backbone bits) whose connection is governed by an harmonic potential, as shown in figure 5.16.

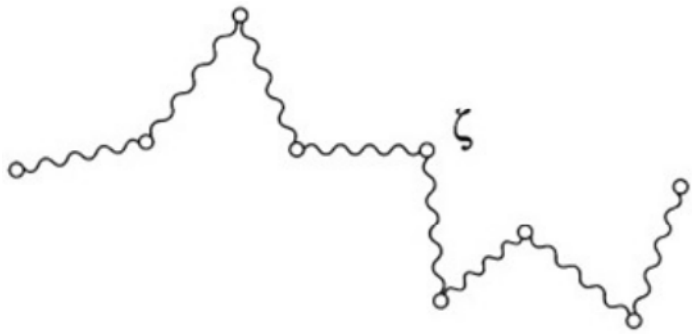

Figure 5.16: The Rouse Model. Backbone bits are connected by an harmonic oscillator. Each backbone bit independately has its own friction coeficient ζ [51].

Given the fact that Rouse Chains have many degrees of freedom, the relaxation process is described by some characteristic relaxation times. The longest of them, is called Rouse relaxation time or longest relaxation time and usually is denoted by the symbol τ_r. Consider again the End to End vector $\overrightarrow{R}_{EtoE}$. According to the Rouse Model, the time autocorrelation function $< \overrightarrow{R}_{EtoE}(t)\,\overrightarrow{R}_{EtoE}(0) >$ is given by the following expression:

$$< \overrightarrow{R}_{EtoE}(t)\,\overrightarrow{R}_{EtoE}(0) > \propto \exp\left(\frac{-t}{\tau_r}\right) \quad \text{for} \quad t \geq \tau_r \tag{5.14}$$

There is also an expression for τ_r:

$$\tau_r = \frac{\zeta N^2 b^2}{3\pi^2 k_B T} \tag{5.15}$$

Where ζ is the friction coefficient, N is the number of the backbone spheres, b is the mean distance between the backbone spheres, k_B is the Boltzmann constant and T is the temperature. From the expression above we observe that there is a linear relation between the friction coefficient and the longest relaxation time.

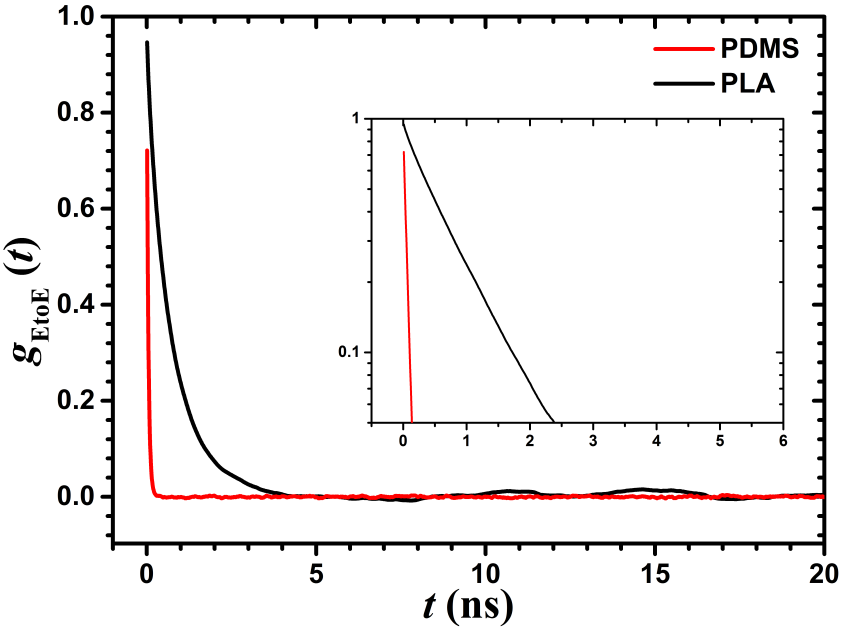

Figure 5.17: The normalized autocorrelation function g_{EtoE} for PDMS (red) and PLA (black).

Both these factors describe the conformational dynamics of a system, however the friction coefficient is more useful because it is independent of the chain's length and as a result constitutes a conformational fingerprint for each polymer.

Computationally, the longest relaxation time and the friction coefficient can be estimated by MD simulations. The trajectories of the first and the last backbone bits for each polymer chain are given for every time step. As a result, the autocorrelation function can directly be estimated and then by the use of equations 5.14 and 5.15. Usually, instead of using the autocorrelation function, it is useful to normalize it, by dividing it with the norm of the vectors $\overrightarrow{R}_{EtoE}(t)$ and $\overrightarrow{R}_{EtoE}(0)$, as follows:

$$g_{EtoE}(t) = \left\langle \frac{\overrightarrow{R}_{EtoE}(t)}{|\overrightarrow{R}_{EtoE}(t)|} \frac{\overrightarrow{R}_{EtoE}(0)}{|\overrightarrow{R}_{EtoE}(0)|} \right\rangle \tag{5.16}$$

The "normalized" autocorrelation function g_{EtoE} apparently satisfies the following expressions:

$$\begin{aligned} g_{EtoE}(0) &= 1 \\ \lim_{t\to\infty}(g_{EtoE}(t)) &= 0 \end{aligned} \tag{5.17}$$

From the previous figure, we observe that PDMS dynamics is extremely fast

since the normalized autocorrelation function adopts the null value from the very first tenths of nanosecond. On the other hand the autocorrelation function for PLA falls more gradually, yielding slower dynamical behaviour. By using equation 5.14 we were able to estimate the longest relaxation time. The results are shown on the following table:

Table 5.4: Estimation of longest relaxation time for PDMS and PLA pentamer melts at atmospheric pressure and a temperarure of 450K. Errors are presented as well.

	PDMS	**PLA**
τ_r (ns)	0.047	0.833
$\delta\tau_r$ (ns)	$1.6 \cdot 10^{-4}$	$7.5 \cdot 10^{-4}$

The estimated longest relaxation time for PDMS is very low as expected from figure 5.17 and this consists a strong indication of a very low glass transition temperature. This can be verified by the experimental and computational results that were presented in the previous section. We observed that PDMS has a very low glass transition temperature (131.7K) compared to PLA (307.8K). At this point we are able to use equation 5.15 in order to estimate the friction coefficient ζ for PDMS and PLA.

5.4.3 Self Diffusion Coefficient

Another important property of polymer melts is the Self Diffusion Coefficient. It reflects the ability of polymer chains to move among other similar chains. In order to estimate the self diffusion coefficient, we should at first define the Center of Mass Autocorrelation function g_3. Before so, we should at first describe the center of mass vector $\overrightarrow{R}_{CM}$:

$$\overrightarrow{R}_{CM} = \frac{\sum_{i=1}^{n} m_i \overrightarrow{r_i}}{\sum_{i=1}^{n} m_i} \tag{5.18}$$

In the expression above, n is the number of atoms. $\overrightarrow{r_i}$ is the vector of the atom i of mass m_i. When performing an MD simulation the center of mass vector is not stable, thus it can be expressed as a function of time ($\overrightarrow{R}_{CM}(t)$). At this point, we may define the Center of Mass Autocorrelation function:

$$g_3(t) = < [\overrightarrow{R}_{CM}(t) - \overrightarrow{R}_{CM}(0)]^2 > \tag{5.19}$$

In the expression above, $\overrightarrow{R}_{CM}(0)$ is the initial center of mass vector. It is obvious that g_3 is the mean square displacement of the center of mass function. According to the Rouse Model, g_3 satisfies the following expression [52]:

$$\lim_{t\to\infty} g_3(t) = 6D_{CM}t \tag{5.20}$$

where D_{CM} is the Self Diffusion Coefficient. Polymers that have higher values of D_{CM} are likely to be self-diffusive. Computationally, the self diffusion coefficient can be estimated by MD simulations. Given the trajectories of each atom that is a part of the polymer chains, it possible to estimate the center of mass of the polymer system for every time step. By plotting the center of mass autocorrelation function over time, we are able to estimate the self diffusion coefficient, by using equation 5.20. For PDMS and PLA the g_3 over time plot is shown in figure 5.18

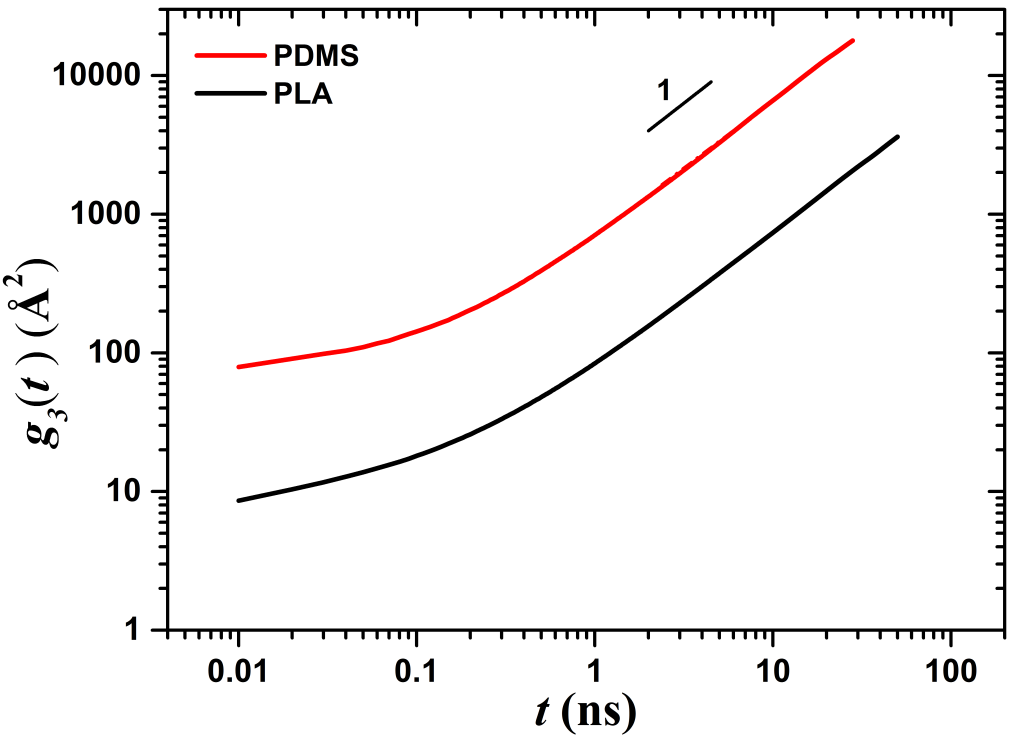

Figure 5.18: The Center of Mass mean square displacement function over time for PDMS (red) and PLA (Black).

On figure 5.18 we observe that the center of mass autocorrelation function for both PDMS and PLA obtains a stable slope after a small period of 1ns. This value of slope equals unity, that is we are allowed to use equation 5.20 in order to estimate the self diffusion coefficient D_{CM}. Our estimations for D_{CM} for both PDMS

and PLA are shown on table 5.5. We found that the PDMS value of D_{CM} is almost ten times higher than the corresponding value of PLA, that is PDMS is more to be self-diffusive. Before finishing the discussion about the self diffusion coefficient, we should also underscore that D_{CM} depends on the degree of polymerization. In this work, we performed MD simulations for oligomer chains which are more likely to be self-diffusive. In the case of longer chains we expect that the self diffusion coefficient would be lower.

Table 5.5: Self Diffusion Coefficient for PDMS and PLA pentamers.

$\mathbf{D_{CM}}$ **[10^{-10} m/s^2]**	
PDMS	PLA
11.1	1.25

5.5 Hildebrand Solubility Parameter

The Hildelbrand solubility parameter δ can be estimated by running a MD simulation and provides an estimate of the degree of interaction between materials. Particulartly for polymers, it can be a good indication of solubility. It is used in the industry to predict the compatibility and swealing between polymers [55]. In order to offer an expression for δ we should at first describe the cohesive energy.

$$E_{coh} = E_{tot.melt} - E_{tot.chain} \tag{5.21}$$

At the previous expression, $E_{tot.melt}$ is the energy of the total melt, $E_{tot.chain}$ is the summation of energy of each chain as a result of intramolecular interactions. In other words, the cohesive energy represents the energy of the total attractive interactions between chains. These forces are presumably the electrostatic and the Wan der Walls interactions. It is equivalent to the amount of energy required to separate the constituent chains to an infinite distance where the melt's potential energy approaches zero. In order to estimate the Hildebrand solubility parameter, we performed MD simulations, and used the following equation:

$$\delta = \sqrt{\frac{< E_{coh} >_{NpT}}{V_{NpT}}} \tag{5.22}$$

The previous expression states that Hildebrand solubility parameter is the square root of the fraction of the cohesion energy to the volume. It consists a way to

measure how strong is the attraction of same chains which are in a melt of volume V. The simulation results compared to the experimental [8], are shown on figures 5.19 and 5.20.

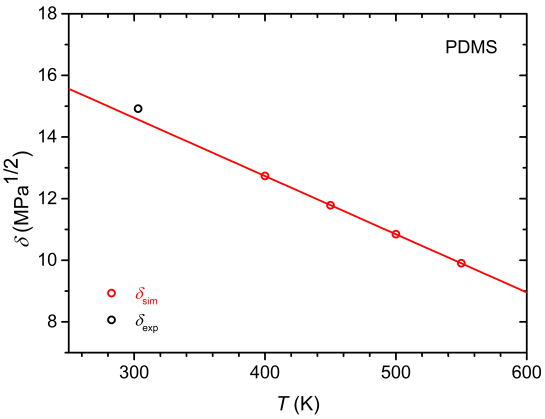

Figure 5.19: Simulation results compared to experimental [8] for the Hildebrand solu-bility parameter for PDMS.

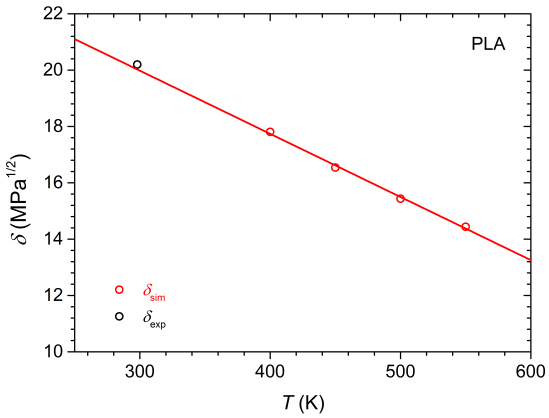

Figure 5.20: Simulation results compared to experimental [8] for the Hildebrand solu-bility parameter for PLA.

We performed four MD simulations for PDMS and PLA melts at 400K, 450K, 500K and 550K. We observed a linear behaviour, an for that reason by using linear regression we tried to compare the simulation results tha were available at 300K. We observed a significant accordance between simulation and experiment.

5.6 Mixing Properties

In this section we study the mixing properties of PDMS and PLA melt. Our primary target is to extract conclusions regarding the immiscibility od PDMS and PLA. This is described by the Flory - Huggins interaction parameter as described in the first chapter. The most important equation for this purpose is eq.1.19:

$$\Delta_{mix}H = \varphi_1\varphi_2 k_B T V \frac{\chi}{v^*}$$

ΔH_m apparently satisfies the expression:

$$\Delta_{mix}H = H_{\text{Blend}} - H_{\text{PDMS}} - H_{\text{PLA}} \tag{5.23}$$

In the previous expression, H_{blend} refers to the enthalpy of the PDMS/PLA blend, H_{PDMS} refers to the enthalpy of the pure PDMS melt and H_{PLA} refers to the enthalpy of the pure PLA melt. By running MD simulations we are able

to estimate ΔH_{blend}, ΔH_{PDMS} and ΔH_{PLA} by using the fundamental expression of enthalpy:

$$\Delta H = \Delta \mathcal{V} + p\Delta V \tag{5.24}$$

All the MD simulations we run in order to estimate χ were at 450K. The enthalpy over time graph for PDMS and PLA is shown on figures 5.21 and 5.22, respectively. The value of v^* is $117.6A^3$ and taken from [44].

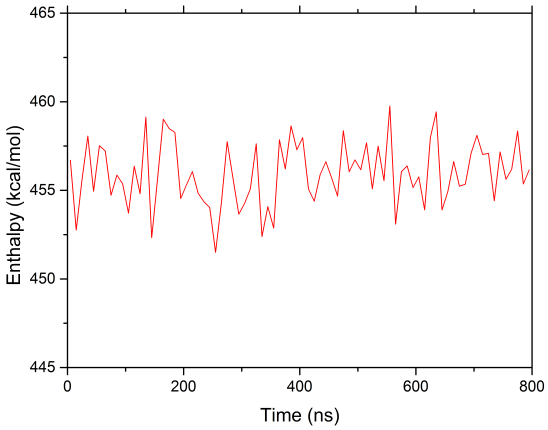

Figure 5.21: Enthalpy over time for one initial configuration for PDMS.

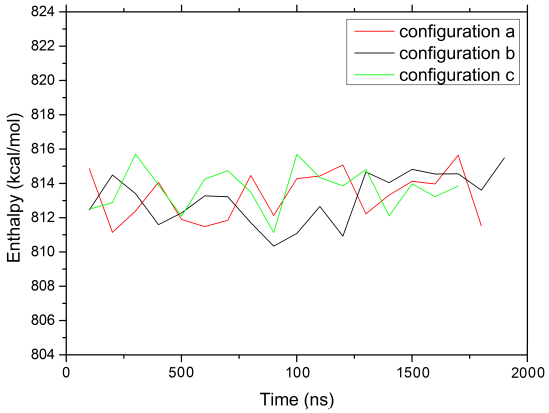

Figure 5.22: Enthaply over time for three initial configurations for PLA.

For PDMS, we estimate the average enthalpy form figure 5.21, after 400ns were the graph's behaviour is less violent. The estimated value of H_{PDMS} is $456.28\frac{kcal}{mol}$. For PLA, we runned MD simulations for three different initial configurations. We observe that the enthalpy for these different configurations is not significantly dissimilar thus the initial configuration of a system does not affect its enthalpy. This is explained by the fact that energy minimization takes place every time we run an MD simulation, as explained on chapter 4. At this point, in order to estimate the H_{blend}, we run an MD simulation for a PDMS/PLA polymer blend, consisting of 10 chains of each polymer. The simulation result for enthalpy over time is shown on figure 5.23.

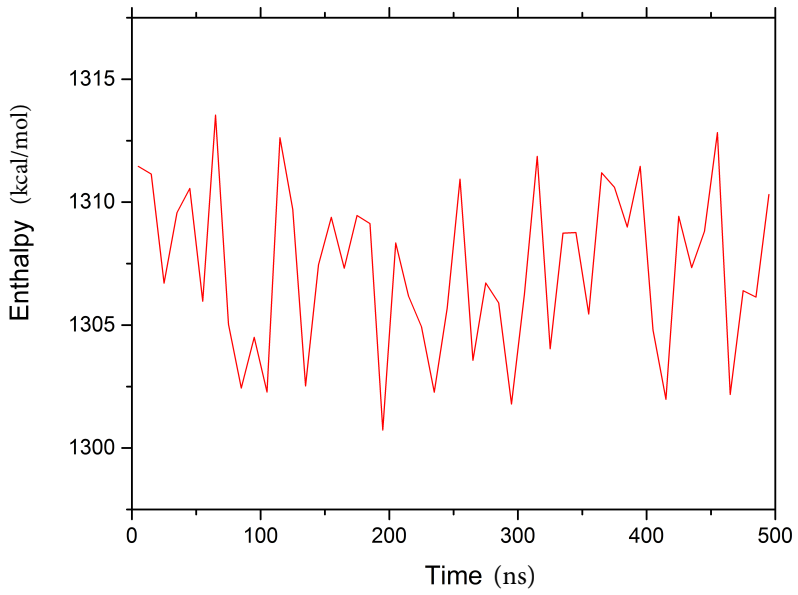

Figure 5.23: Enthalpy over time for three initial configurations for PDMS/PLA blend.

From the previous graph, the average value of enthalpy is estimated 914.32$\frac{kcal}{mol}$. We are ready at this point to employ equation 1.19 in order to estimate the value of χ. The result is 1.34 and for $\Delta_{mix}H$ is 62.87kcal/mol. The interchange energy density ($\frac{\chi}{v^*}$) is estimated $0.011A^{-3}$. Rodwogin et at [29] at their work suggested that temperature dependence of χ for the PDMS/PLA blend satisfies the following empirical expression:

$$\chi = \frac{360}{T} + 0.21 \tag{5.25}$$

At 450K, the value of according to the previous expression equals 1.01 which is different from the value he have estimated. We expected to experience such a discord, since the force field we used in order to run the MD simulation was made to describe the separate melts of PDMS and PLA, and not their blend.

Since the force field we used fails to describe the miscibility of the system, there is an urgent need to parametrize it. In order to make a force field that would accurately reproduce the mixing property of the blend, we should modify the Lennard-Jones parameters that refer to the intermolecular interactions between different chains. The whole parametrization process will be guided by the following expression:

$$\varepsilon_f = (1 - \lambda)\varepsilon_i \tag{5.26}$$

At the previous expression, ε_i refers to the initial value of the depth of the potential well of the Lennard-Jones potential and ε_f refers to the final value which will

be used as an input to the forcefield. The central factor of the parametrization is λ. In order to overcome the problem that emerged before and to make a new force field that would describe accurately the miscibility of the blend, we should find the appropriate value of λ that would finally lead to a correct estimation of the χ parameter. The whole process of the parametrization will be reinforced by a graph which will demonstrate the dependence of χ to λ. We initially performed two MD simulations for λ values 0.1 and -0.1. The results are shown on figure 5.24

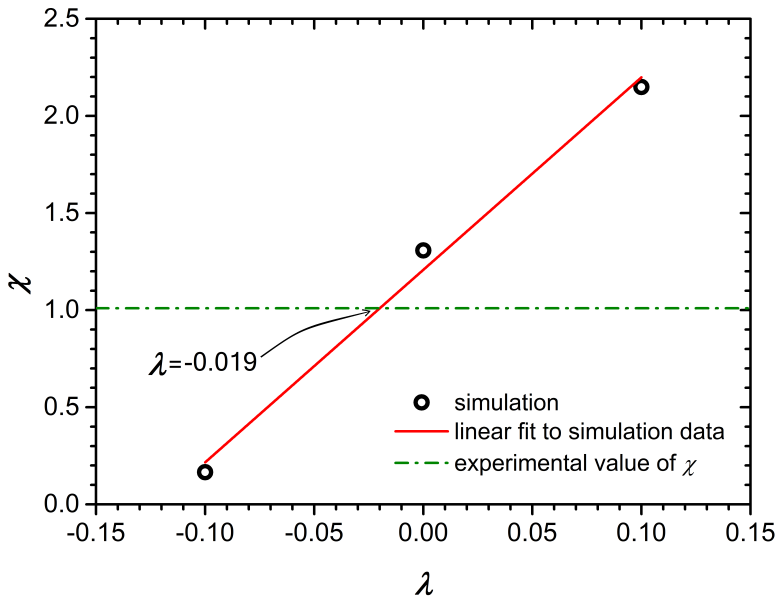

Figure 5.24: Dependence of χ on λ.

In order to estimate the value of λ that leads to the desirable value of χ which is 1.01, we employed linear interpolation since we observed from the previous graph a linear dependence of χ on λ. According to the graph then, we observe that the value of λ that would probably lead to the target experimental value of χ at 1.01 is -0.019. In order to validate the previous parametrization and run a new simulation MD simmulation for 800ns using the ε values for the depth of Lennard-Jones potential as described in equation 5.26. The time dependence of enthalpy for the new simualtion is given on figure

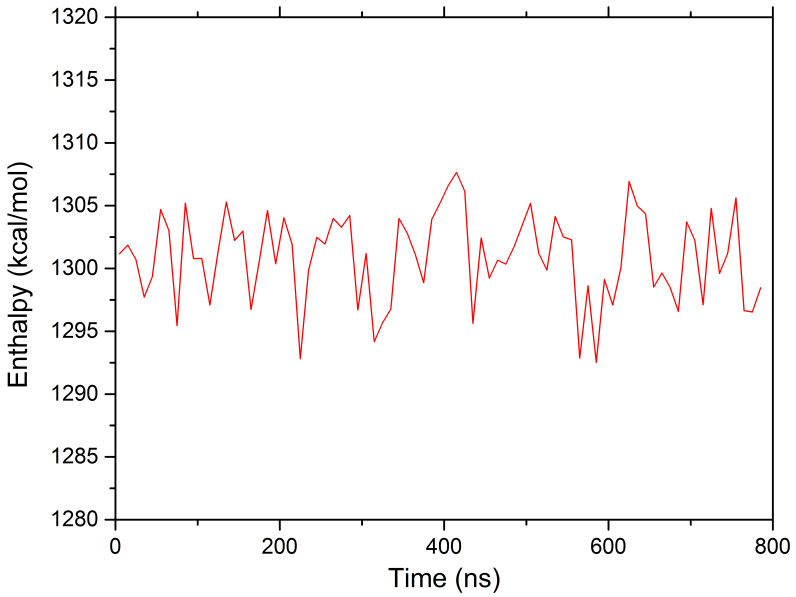

Figure 5.25: Enthalpy over time for $\lambda = -0.019$.

The enthalpy is estimated $1300.53\frac{kcal}{mol}$. We used this value as an input to the equation 1.19 and the new value of χ is estimated 1.07 which is very close to the target experimental value. That is, our parametrization was successful. $\Delta_{mix}H$ is estimated as 29.93kcal/mol and the interchange energy density 0.0089. The Final graph of dependence of χ on λ is shown on figure 5.26.

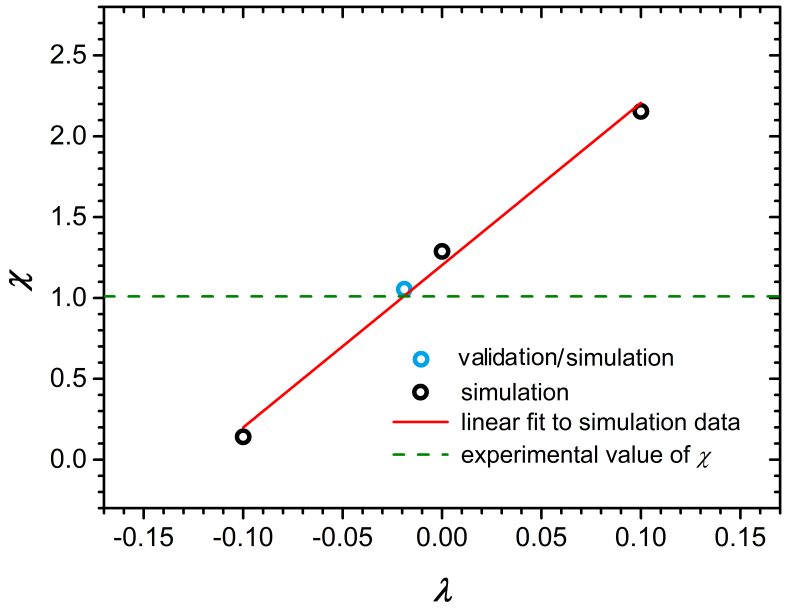

Figure 5.26: Dependence of χ on λ with the validation of the parametrization.

We should somehow provide an interpretation of the previous figure. The general observation is that low values of λ lead to low values of χ. Lets consider a simple system of A and B spheres. The system's interactions are only governed by Lennard-Jones potentials. An increase of λ leads to smaller values of the well depth ε_i, as described in equation 5.26 and the depth is moved upwards. Oppositely, a decrease of λ leads to an increase of the ε_i, that is the L-J potential has a deeper well and the interactions between the different spheres are favoured. All the above are qualitatively shown on figure 5.27. When the well is not very

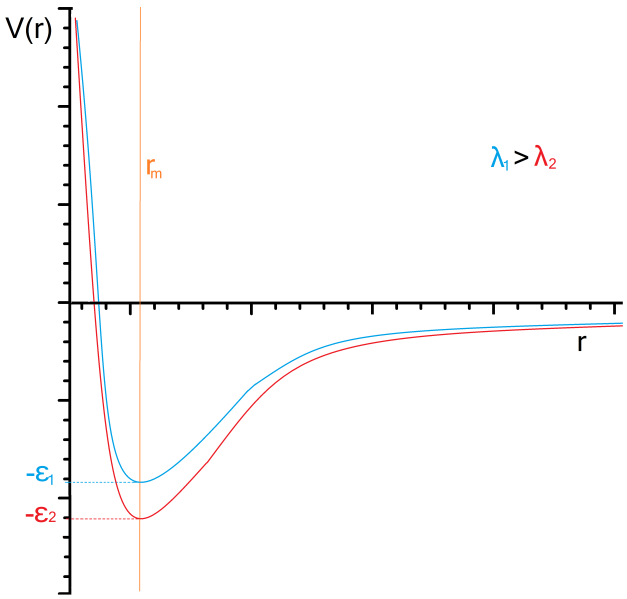

Figure 5.27: Qualitative representation of the dependence of the well's value on λ.

deep (as in the case of ε_1), interactions between A and B spheres are not intensive, and thus they are more likely to separate. On the other hand, deep Lennard Jones wells favour the interactions between the different spheres and the separation between them is not likely to happen, so the χ parameter is expected to obtain low values. To make a conclusion that would interpret figure 5.26 we should state that low values of λ lead to less interactions between different materials and thus, the χ parameter is decreased.

CHAPTER 6

Epilogue

6.1 Contribution

In this work, many topics regarding the self assembly of block copolymers have been covered. Elegant equations that have been part of the Flory - Huggins theory, provide an avenue of describing in thermodynamic and mathematical terms the appearance of self-assembly in domains of block copolymers. The significant importance of this theory was a main reason to award Flory the Nobel Prize in chemistry in 1974. This theory has been used a lot over the past decades in order to extract valuable information regarding the miscibility of different materials.

A great part of this work was based on Flory's theory for estimating the χ parameter by simulation methods. The spearhead of this work was the successful parametrization of the PDMS/PLA blend forcefield. By accomplishing this parametrization we generated a force field that is able to efficiently describe the immiscibility between PDMS and PLA. Since the PDMS-b-PLA is considered to revolutionize the DSA of Block Copolymers for lithography applications, the new force field will give the opportunity to study other important properties by employing computational material science methods.

Apart from the χ factor, a lot of effort has been made to study other properties and to compare the simulation results to available experimental data. By doing this comparison, we were able to validate the force fields that we used. In most cases, simulation results were in accordance with the experimental and that is indication that the force fields were able to describe accurately and efficiently

the systems that we studied. Many properties of the PDMS and PLA melts have been studied by this work. Volumetric, solubility, conformational and dynamical properties were estimated by molecular dynamics and monte carlo simulations. All of these properties are of great importance and they will play a central role in guiding the selection of suitable and novel materials for DSA applications.

6.2 Future Plans

Many steps are yet to be taken in order to push DSA to the forefront of lithography. The two experimental methods, graphoepitaxy and chemical epitaxy, that are used to direct the self assembly of block copolymers should overcome many difficulties, since they are in at an early stage of development. The whole procedure though will be enhanced by novel materials, and the PDMS-b-PLA blend consists one of them.

The successful parametrization of the force field of PDMS/PLA blend gives the opportunity to extend the computational study of these materials and to deliver answers regarding their potential use in DSA for lithography applications. A first step after the parametrization is the computational study of the dependence of χ factor on the volume fractions of the two polymers. Diffusivity between the two polymers could be studied, delivering valuable information regarding their potential use in DSA.

Another work that would also benefit from the parametrization we made, is the estimation of the stiffness of PDMS-b-PLA by single chain Monte Carlo simulations. Having estimated the stiffness the Kuhn's length could be studied as well. MD simulations could also be employed in order to study the phase separation of PDMS-b-PLA which is of great importance for lithography because it is directly associated with the essential geometries that are fabricated.

Last but not least, another future work should also be underscored before closing the chapter. At this work we simulated oligomer melts of PDMS and PLA in order to study their miscibility by estimating the χ factor. We did so just by considering only the enthalpic affects. There is also an entropic affect to the χ factor. As stated in equation 1.24 the two terms (enthalpic and entropic) that affect the χ factor are given by the following expression:

$$\chi = \frac{A(\varphi)}{T} + B(\varphi)$$

The structure of the system, which is an input to estimate the entropy, affects the free energy of mixing, and this is described by the second term of the previous

expression, whereas the first one refers to the dependence of the free energy to enthalpy. Efforts should be made in order to integrate the entropic term at the computational study as well.

Appendix

In the following tables Oe stands for ester oxygen molecules, the indication bn refers to backbone atoms and the indication Ocb to oxygen carbonyls.

Table A1: Lennard Jones Interraction Parameters for PLA

ε_{ij}	σ_{ij}	**Interraction Type**
0.020	4.680	CH CH
0.040	4.290	CH Cbn
0.062	4.215	CH CH_3
0.047	3.740	CH Oe
0.056	3.865	CH Obn
0.043	4.315	CH CH_2
0.081	3.900	Cbn Cbn
0.126	3.825	Cbn CH_3
0.094	3.350	Cbn Oe
0.113	3.475	Cbn Obn
0.086	3.925	Cbn CH_2
0.195	3.750	CH_3 CH_3
0.146	3.275	CH_3 Oe
0.175	3.400	CH_3 Obn
0.133	3.850	CH_3 CH_2
0.109	2.800	Oe Oe
0.131	2.925	Oe Ocb
0.100	3.375	Oe CH_2
0.157	3.050	Ocb Ocb
0.120	3.500	Ocb CH_2
0.091	3.950	CH_2 CH_2

Table A2: Lennard Jones Interraction Parameters for PDMS at 450K

ε_{ij}	σ_{ij}	**Interraction Type**
0.1310	4.290	Si Si
0.1596	4.010	Si Obn
0.0772	3.940	Si CH_3
0.1944	3.730	Obn Obn
0.1247	3.515	Obn CH_3
0.0800	3.300	CH_3 CH_3

In the two following tables, e stands for the charge of an electron which is equal to $-1.602176565 \cdot 10^{-19}$ C.

Table A3: Charges of PDMS molecules

Molecule	**Charge (e)**
Si	0.30
Obn	-0.30

Table A4: Charges of PLA molecules

Molecule	**Charge (e)**
CH_2	0.10
CH	0.15
C	0.40
Obn	-0.40
Ocb	-0.25

Table A5: a_l, τ_l, t_s, β and t_c parameters for various temperatures for PDMS

T (K)	$\mathbf{a}_l$	$\boldsymbol{\tau}_l$	$\mathbf{t}_s$	β	$\mathbf{t}_c$
200	-0.37000	2.06000	2.91800	0.56000	5.86013
220	-0.20650	0.47281	0.56498	0.53065	1.13110
240	-0.14130	0.06923	0.11970	0.52612	0.24002
260	-0.10157	0.01838	0.04939	0.51547	0.10116
280	-0.03680	0.26255	0.03279	0.53500	0.05081
300	0.06800	0.03479	0.01695	0.53406	0.03054

Table A6: a_l, t_l, t_s, β and t_c parameters for various temperatures for PLA

T (K)	$\mathbf{a}_l$	$\mathbf{t}_l$	$\mathbf{t}_s$	β	$\mathbf{t}_c$
400	0.24460	2.01153	0.26292	0.39789	1.16181
410	-0.37801	0.21046	0.28536	0.53322	0.62367
425	-0.18904	0.61572	0.09577	0.41584	0.22483
450	0.24572	0.00279	0.11042	0.64693	0.11508
475	0.18946	0.0979	0.01747	0.43942	0.05561
500	-0.19677	0.01304	0.01630	0.53941	0.03161
525	0.14329	0.03789	0.00780	0.48310	0.01970
550	-0.04893	0.09443	0.00915	0.50799	0.01403

Bibliography

[1] R. H. Colby, "Breakdown of time-temperature superposition in miscible polymer blends ", *POLYMER, Vol 30, 1989.*

[2] J. Parameswaranpillai, S. Thomas, and Y. Grohens, "Characterization of Polymer Blends: Miscibility, Morphology and Interfaces" *Whiley Online Library, 2014*.

[3] B. Andersen Dissertation, "Investigations on Environmental Stress Cracking Resistance of LDPE/EVA Blends", *Martin-Luther-Universität Halle-Wittenberg, Germany 2004*.

[4] U. Eisele, "Introduction to Polymer Physics", *Springer Verlag, Heidelberg 1990*.

[5] T. E. Raptis, V. E. Raptis, "Understanding coil-to-globule transition of polymers with the aid of a novel cluster analysis technique", *Condensed Matter, 2013*

[6] NIST Center for Neutron Research
`https://www.ncnr.nist.gov/staff/hammouda/distance_learning/`

[7] G. M. Whitesides and B. Grzybowski, "Self Assembly at All Scales" , *Science AAAS 2012.*

[8] J. E. Mark, "Physical Properties of Polymers Handbook", *Springer Publications 2007.*

[9] S.B. Darling, "Directing the self-assembly of block copolymers", *Elsevier Prog. Polym. Sci. 32 1152–1204 2007.*

[10] F. S. Bates, G. H. Fredrickson, "Block copolymers—designer soft materials", *Phys Today 52:32–8, 1999*.

[11] G. H. Fredrickson', A. J. Liu and F. S. Bates, "Entropic Corrections to the Flory-Huggins Theory of Polymer Blends: Architectural and Conformational Effects ", *Macromolecules 27, 2503-2511, 1994*.

[12] A. Pimpin and W. Srituravanich, "Review on Micro- and Nanolithography Techniques and their Applications", *ENGINEERING JOURNAL Volume 16 Issue 1, 2012*.

[13] C. M. Bates, M. J. Maher, D. W. Janes, C. J. Ellison and C. Grant Willson, "Block Copolymer Lithography", *ACS publications, Macromolecules, 2013*

[14] Y. C. Tseng and S. B. Darling, " Block Copolymer Nanostructures for Technology", *Polymers 2, 470-489, 2010*.

[15] A. R. Leach, "Molecular Modeling: Principles and Applications", *Prentice Hall, second edition 2001*.

[16] Metropolis N., Rosenbluth A.W., Rosebluth M.N.; Teller, A.H. Teller, E. J., *Chem. Phys. 21, 1087, 1949*.

[17] M. P. Stoykovich, H. Kang, K. Ch. Daoulas, G. Liu, C. C. Liu, J. J. de Pablo, M. Müller, and P. F. Nealey, "Directed Self-Assembly of Block Copolymers for Nanolithography: Fabrication of Isolated Features and Essential Integrated Circuit Geometries", *ACSNano, vol.1, NO.3, 2007.*

[18] Jung Y. and Ross C., "Orientation-Controlled Self Assebled Nanolithography Unising a POlystyrene - Polydimethylsiloxane Block Copolymer", *ENano Lett. 7, 2046 2007.*

[19] J. D. Plummer, M. Deal and P. D. Griffin, "Silicon VLSI Technology: Fundamentals, Practice, and Modeling", *Prentice Hall Publications, 2000*.

[20] R.W. Dyson, Ed. Chapman, "Specialty Polymers", *New York, NY 1987*.

[21] A. Rösler, G. W. M. Vandermeulen, H. A. Klok, "Advanced drug delivery devices via self-assembly of amphiphilic block copolymers", *Advanced Drug Delivery Reviews, Elsevier, 2012.*

[22] Y. Zhou , W. Huang , J. Liu , X. Zhu , and D. Yan, "Self-Assembly of Hyperbranched Polymers and Its Biomedical Applications" *Advanced Materials, 2010.*

[23] D. N. Theodorou, "Applied Molecular Theory for Engineers", *NTU Athens, 2004*.

[24] E. M. Furst, "Directed Self Assembly", *RSC Publishing, Soft Matter, 2013.*

[25] C. Park, J. Yoon, E. L. Thomas, " Enabling nanotech-nology with self assembled block copolymer patterns", *Elsevier Polymer 2003.*

[26] S. J. Jeong, S. M. Kim, J. E. Kim, J. B. Kim, H. S. Moon and S. O. Kim, " Soft Graphoepitaxy of Block Copolymer Assembly with Disposablr Photoresist Confinement", *NANO LETTERS Vol. 9, No. 6 2300-2305, 2009.*

[27] J. C. Lotters, W. Olthuis, P. H. Veltink and P. Bergveld, "The mechanical properties of the rubber elastic polymer polydimethylsiloxane for sensor applications", *IOP SCIENCE, 1997.*

[28] D. C. Duffy, J. C. McDonald, O. J. A. Schueller and G. M. Whitesides, "Rapid prototyping of microfluidic systems in poly(dimethylsiloxane)", *Analytical Chem 1998.*

[29] M. D. Rodwogin, C. S. Spanjers, C. Leighton and M. A. Hillmyer, "Polylactide - Poly(dimethylsiloxane)-Polylactide Triblock Copolymers as Multifuntional Materials for Nanolithographic Applications", *ACS Nano, VOL4. NO.2 725-732, 2010.*

[30] K. A. Maerzke, N. E. Schultz, R. B. Ross and J. I. Siepmann, "TraPPE-UA Force Field for Acrylates and Monte Carlo Simulations for Their Mixtures with Alkanes and Alcohols", *J. Phys. Chem. B, 113, 6415–6425, 2010.*

[31] J. M. Stubbs, J. J. Potoff, and J. I. Siepmann, "Transferable Potentials for Phase Equilibria. 6. United-Atom Description for Ethers, Glycols, Ketones, and Aldehydes", *J. Phys. Chem. B, 108, 17596-17605, 2004.*

[32] S. Clifford, K. Bolton, and D. Ramjugernath, "Monte Carlo Simulation of Carboxylic Acid Phase Equilibria", *J. Phys. Chem. B, 110, 21938-21943, 2006*.

[33] A. Habenschuss, M. Tsige, J. G. Curro, G. S. Grest and S. K. Nath, "Structure of Poly(dialkylsiloxane) Melts: Comparisons of Wide-Angle X-ray Scattering, Molecular Dynamics Simulations, and Integral Equation Theory", *Macromolecules 40, 7036-7043, 2007*.

[34] M. Rubinstein, R. H. Colby, "Polymer Physics", *Oxford Press 2004*

[35] http://scienomics.com/products/molecular-modeling-platform

[36] http://what-when-how.com/nanoscience-and-nanotechnology/

[37] S. K. Sia and G. M. Whitesides, "Microfluidic devices fabricated in poly(dimethylsiloxane) for biological studies" *Electrophoresis 2003.*

[38] J. Y. Cheng, C. T. Rettner, D. P. Sanders, H. C. Kim, and W. D. Hinsberg, "Dense Self-Assembly on Sparse Chemical Patterns: Rectifying and Multiplying Lithographic Patterns Using Block Copolymers", *Advanced Materials, 20, 3155–3158, 2008.*

[39] C. T. Black, "Polymer Self Assembly as a Novel Extension to Optical Lithography", *ACS Nano, Vol.1 No.3 147-150, 2007.*

[40] Xiao et al, "Graphoepitaxy of cylinder-forming block copolymers for use as templates to pattern magnetic metal dot arrays", *IOP Science Nanotechnology, 2005*.

[41] G. S. Doerk, C. C. Liu, J. Y. Cheng, C. T. Rettner, J. W. Pitera, L. E. Krupp, T. Topuria, N. Arellano, and D. P. Sanders, "Pattern Placement Accuracy in Block Copolymer Directed Self-Assembly Based on Chemical Epitaxy", *ACS Nano VOL.7 NO. 1 276–285, 2013*

[42] R. Auras, L. T. Lim, S. M. Selke, and H. Tsuji, "POLY(LACTIC ACID) Synthesis, Structures, Properties and Applications", *Wiley Publications, 2010.*

[43] T. Fukuda, M. Nagata, and H. Inagaki, "Light Scattering from Ternary Solutions. 1. Dilute Solutions of Polystyrene and Poly(methy1 methacrylate)", *Macromolecules Vol. 17, 548-553, 1984.*

[44] Rheological properties of amorphous and semicrystalline polylactic acid polymers, "Q. Fang , M. A. Hanna", *Industrial Crops and Products 10 47–53, 1999.*

[45] I. C. Sanchez, "Relationships between polymer interaction parameters", *Elsevier - Polymer, 1989.*

[46] T. Shiomi, K. Kohno, K. Yoneda, T. Tomita, M. Miya, and K. Imai, "Thermodynamic Interactions in the Poly(viny1 methyl ether)-Polystyrene System", *Macromolecules, 18, 414-419 1985.*

[47] C. J. Clarke, A. Eisenberg, J. La Scala, M. H. Rafailovich, J. Sokolov, Z. Li, and S. Qu, A. Schwarz and Y. Strzhemechny and B. B. Sauer, "Measurements of the Flory-Huggins Interaction Parameter for Polystyrene-Poly(4-vinylpyridine) Blends", *Macromolecules Vol. 30, 4184-4188 1985.*

[48] D. N. Theodorou, Notes for the graduate course "Micro and Macro Level Simuations" of master's "Microsystems and Nanodevices", *2015*

[49] T. I. Morrow and E. J. Maginn*, "Molecular Dynamics Study of the Ionic Liquid 1-n-Butyl-3-methylimidazolium Hexafluorophosphate", *J. Phys. Chem. B, 106, 12807-12813, 2002*

[50] A. Zirkel, V. Urban, D. Richter, L. J. Fetters, J. S. Huang, R. Kampmann, N, Hadjichristidis, "Small-Angle Neutron Scattering Evaluation of the Temperature Dependence of Atactic Polypropylene and Poly(1-butene) Chain Dimensions in the Melt", *Macromolecules vol 25, 6148-6155, 1992*

[51] S. Anogiannakis' PhD Thesis, "Υπολογιστική μελέτη της δυναμικής δικτύων διαπλοκών σε πολυμερικά τήγματα", *National Technical University of Athens, 2012.*

[52] M. Doi and S. F. Edwards, "The Theory of Polymer Dynamics", *CLARENDON Press. Oxfords, 1986*.

[53] M. O. Omelczuk and J. W. McGinity, "The influence of Polymer Glass Transition Temperature and Molecular Weight on Drug Release from Teblets containing Poly(DL-Lactic Acid)", *Pharmaceutical research, Vol 9, 1992.*

[54] K.U. Kirst, F. Kremer, T. Pakulal), and J. Hollingshurst, "Molecular dynamics of cyclic and linear poly(dimethylsiloxanes)", *Colloid Polym. Sci. 272:1420-1429 1994.*

[55] M. D. Shirsat, M. A. Bangar, M. A. Deshusses, N. V. Myung, "Polyaniline nanowires-gold nanoparticles hybrid network based chemiresistive hydrogen sulfide sensor", *Applied Physics Letters vol. 94 (083502):1–3, 2009*.

[56] G. G. Vogiatzis, D. N. Theodorou, "Local Segmental Dynamics and Stresses in Polystyrene–C60 Mixtures", *Macromolecules 47 (1), 387-404, 2013*

[57] M. Roth, "Solubility parameter of poly(dimethyl siloxane) as a function of temperature and chain length", *Jurnal of Polymer Science, Part B, 1990*

[58] R. Aura, L.-T. Lim, S. E.M. Selke, and H. Tsuji, "Poly(Lactic Acid) Synthesis, Structures, Properties, Processing and Application", *New Jersey, Wiley, 2010*